

國立臺灣大學電機資訊學院電機工程學系



博士論文

Department of Electrical Engineering

College of Electrical Engineering and Computer Science

National Taiwan University

Doctorial Dissertation

利用擴散張量成像區分梗塞中心與缺血半影區：

動物模型

Differentiation of the Infarct Core from Ischemic
Penumbra using Diffusion Tensor Imaging: A Rat Model

郭敦邦

Duen-Pang Kuo

指導教授：鍾孝文 博士、陳震宇 教授

Advisor: Hsiao-Wen Chung, Ph.D.

Cheng-Yu Chen, M.D.

中華民國 106 年 1 月

January, 2017



國立臺灣大學博士學位論文
口試委員會審定書

利用擴散張量成像區分梗塞中心與缺血半影區：

動物模型

Differentiation of the Infarct Core from Ischemic
Penumbra using Diffusion Tensor Imaging: A Rat Model

本論文係 郭敦邦 君 (d95921026) 在國立臺灣大學電機工程學系、所完成之博士學位論文，於民國 106 年 1 月 13 日承下列考試委員審查通過及口試及格，特此證明

口試委員：

羅若文

(簽名)

陳新 (指導教授)

王福年

彭家勳

吳廷廷

詹宗輝

蔡尚志

高占坤

林春山

系主任、所長

劉志文

(簽名)




中文摘要

急性缺血性中風佔所有中風型態約 80%，主要是因為供應腦組織血流的血管阻塞而引起的，會造成病人死亡或癱瘓。若沒有及時將阻塞血管的血栓打通，缺血半影區(尚存活著的腦組織)將逐漸消失並轉變成不可逆的梗塞中心。1995 年，美國國家神經及中風疾病研究院的研究報告指出：發生急性缺血性中風後 3 小時內，使用靜脈注射血栓溶解劑治療可以有效地改善病人的神經功能並得到有利的治療結果。近年來，更有臨床試驗（例如 ECASS-III，SITS-ISTR）指出病人可以在發病後 3 至 4.5 小時內使用血栓溶解治療，亦可從中獲得治療效果。不幸的是，大多數中風病人，其確切的發病時間是不確定的，將會被排除在血栓溶解治療之外。

此外，在進行任何形式的血栓溶解治療之前，確定是否存在相當體積且能被救活的腦組織，也是一個重要的考量。對於不知道發病時間且將被排除在治療之外的病人，若能考量到其中風情況(例如：存在能救活組織的多寡)，而不單以發病時間作為唯一考量，應可使血栓溶解治療嘉惠更多病人。而現今的造影科技例如電腦斷層攝影或磁振造影，都可幫助臨床醫生藉由影像選出適合血栓溶解的病人。在磁振造影的成像技術中，擴散加權成像和灌注加權成像是可用於評估是否存在能被救活的組織的技術。利用灌注與擴散影像不匹配的概念，臨床醫生可以找出尚存活著組織的多寡，參考並評估超過治療時限的病人是否也能接受溶栓治療。然而，在臨床實務上，病人能接受治療的時間非常急迫，目前的磁振造影後處理決定半影區的方法耗時耗力，對於病人時常緩不濟急，時間是關鍵，任何診斷方法必須快速地完成。

近年來，磁振造影的另一種成像技術，如擴散張量成像，已經成為研究缺血性中風的有利的工具。擴散張量成像能夠描繪出因缺血性中風所導致腦部微結構的細微變化，通常可用擴散張量的非等向性(fractional anisotropy, FA)來表示。在此



研究中，我們認為缺血半影區和梗塞中心血流缺損不同，所引起的細胞損傷也應不同，所反映的 FA 是否也不同?是否可區分缺血半影區和梗塞中心?我們也進一步假設 FA 的變化可以用於推測中風的發病時間。為驗證假設，我們在 7T 磁振造影中建立大鼠永久中大腦動脈梗塞的模型，並重複擴散張量成像序列，分別觀察缺血半影區和梗塞中心 FA 的變化。另一方面，由於 FA 是由純擴散非等向性 (pure anisotropic diffusion, q) 和擴散強度 (diffusion magnitude, L) 的比例來定義，我們也分開研究 q 和 L 以更完整地描述缺血性中風環境的微結構變化。也測試了在純氧環境下 q 和 L 隨時間的變化。結果發現，可以利用 L 值的來區別缺血半影區和梗塞中心。此外，與正常半腦側相比， q 值減少若小於 44.6% 可推測中風發生時間小於 4.5 小時。

我們的結論是，擴散張量成像可以快速且可靠的利用 L 值來區別缺血半影區和梗塞中心，並利用 q 值來估計中風時間，可提供臨床醫生在進行血栓溶解或要保守治療的參考資訊。


關鍵詞：急性缺血性中風；缺血半影區；梗塞中心；擴散加權成像；灌注加權成像；擴散張量成像

Abstract



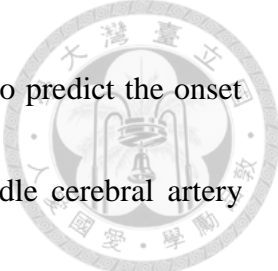
Acute ischemic stroke (AIS), which constitutes approximately 80% of overall strokes, is a major cause of death and disability due to blockage of blood supply to the brain tissue. Without early recanalization, the ischemic penumbra (IP) (i.e., the area that is at risk for infarction) will gradually diminish and then turn into irreversible infarct core (IC) with time. In 1995, the National Institute of Neurological Disorders and Stroke (NINDS) study group reported that treatment with intravenous recombinant tissue plasminogen activator (rtPA) within 3 hours of the onset of AIS can effectively improve the patients' neurological function and result in a favorable outcome at 3 months. In recent years, there have been a number of clinical trials (e.g. ECASS-III, SITS-ISTR) investigating the therapeutic time window beyond 3 of the onset of AIS. For a subgroup of patients with AIS, for example, wake-up stroke, the exact time of onset is uncertain and then would be excluded from rtPA treatment.

In addition, an important consideration is to determine whether the substantial salvageable brain tissue is present before any form of thrombolytic therapy. For patients excluded from rtPA treatment according to current guidelines, the selection of patients for thrombolysis may be made more efficacious by considering individual salvageable



tissue rather than relying solely on the onset time as the determinant of selection. The current imaging modality such as computed tomography (CT) or magnetic resonance imaging (MRI) can comprehensively detect and characterize AIS to help physicians with the selection of appropriate candidates for thrombolysis. In MRI techniques, diffusion-weighted imaging (DWI) and perfusion-weighted imaging (PWI) are two powerful techniques used to evaluate whether the salvageable brain tissue is present. With the use of concept of PWI/DWI mismatch of greater than 20%, clinicians can define the salvageable tissue, which may be considered for selecting patients eligible for thrombolysis beyond time windows. However, the image data processing could be very time-consuming and might not be appropriate in the AIS setting. Because time is critical, an effective diagnostic imaging method is desirable for clinical decision-making.

In recent years, another imaging technique of MRI such as diffusion tensor imaging (DTI) has emerged as a promising tool to study AIS. DTI has shown to be capable of delineating in the micro-structural changes of brain due to ischemic stroke-induced damage, commonly expressed as the fractional anisotropy (FA). In this study, we first hypothesize that the DTI metric changes may differ in IP and IC regions due to ischemic injury as a result of different extents of perfusion deficit. We further



hypothesize that the evolution of DTI metric changes may be used to predict the onset time of AIS. To verify hypotheses, we established permanent middle cerebral artery occlusion (MCAo) model in rat at 7T MRI and then DTI sequences were performed repeatedly after MCAo for longitudinal observation of FA changes from IP and IC, respectively. Because the FA is a relative scalar value defined by the ratio of pure anisotropic diffusion (q) and diffusion magnitude (L), we measured the parameters q and L separately in affected ipsilateral and unaffected contralateral sides and calculated differences between the ipsi- and contralateral side (r) for more complete picture of diffusion changes in AIS. We also test the effect of oxygenation in the evolution of q and L . The study found that discrimination of IP from IC by rL values showed comparable results to the conventional PWI/DWI mismatch. Additionally, by regression analysis, the stroke age of 4.5 hours can be estimated by an r_q value of -44.6% (a 44.6% reduction) in the cortical IC regions.

In conclusion, our preliminary results suggest that a single DTI could provide a quick and reliable measure to distinguish IP from IC based on the L values, and estimate stroke age using the q values, thus potentially provide valuable information to the treating physicians considering whether to treat acute stroke by means of

thrombolytic therapy or conservative management.



Keywords: acute ischemic stroke; ischemic penumbra; infarct core; diffusion-weighted imaging; perfusion-weighted imaging; diffusion tensor imaging

目錄



口試委員會審定書	
中文摘要.....	i
英文摘要.....	iii
List of figures.....	ix
List of tables.....	x
Chapter 1 Introduction	
References.....	1-5
Chapter 2 Methods	
2.1 Diffusion tensor imaging and the anisotropy index.....	2-1
2.2 Dynamic susceptibility contrast-enhanced technique.....	2-10
2.3 Topographic classification of brain tissue types.....	2-15
2.4 References.....	2-22
Chapter 3 Using DTI metrics in animal stroke model	
3.1 stroke model in normobaric hyperoxia.....	3-1
3.1.1 Introduction.....	3-1
3.1.2 Animal preparation and data analysis	3-4
3.1.3 Results.....	3-9
3.1.4 Discussion and conclusion.....	3-12
3.2 stroke model in room air	3-26
3.2.1 Introduction.....	3-26
3.2.2 Animal preparation and data analysis.....	3-27
3.2.3 Results.....	3-31

3.2.4 Discussion and conclusion.....	3-32
3.3 References.....	3-35
Chapter 4 Conclusion	





List of figures

Fig. 1-1. The definition of the temporal parameters the diffusion gradient.....	2-8
Fig. 1-2. Schematic representation of diffusion ellipsoid.....	2-8
Fig. 1-3. Conventional T2 images and the corresponding ADC and FA maps of a rat stroke model.....	2-9
Fig. 1-4. Dynamic contrast-enhanced MR imaging of a rat brain.....	2-13
Fig. 1-5. Color-coded hemodynamic maps of an embolic stroke rat.....	2-14
Fig. 1-6. The FA templates of Sprague-Dawley rat brain and the corresponding atlas delineations.....	2-18
Fig. 1-7. Atlas-based classification process using FLIRT toolbox.....	2-19
Fig. 1-8. The spatial maps of identified tissue subtypes.....	2-20
Fig. 2-1. Serial L, q, FA, and T2WI maps of an embolic stroke rat.....	3-20
Fig. 2-2. Temporal evolutions of DTI metrics in tissue subtypes.....	3-21
Fig. 2-3. ROC curves in discriminating IP from IC and NT.....	3-22
Fig. 2-4. Comparison of perfusion-diffusion mismatch with proposed L-defined ...	3-23
Fig. 2-5. Relationship between the rq value and the time after stroke for the cortical IC.....	3-24
Fig. 2-6. Representative perfusion/diffusion mismatch.....	3-25
Fig. 2-7. Temporal evolutions of relative L values in tissue subtypes.....	3-34
Fig. 2-8. Temporal evolutions of relative q values in tissue subtypes.....	3-34

List of tables



Table 1-1. The cerebral regions defined in Sprague Dawley rat brain atlas.....2-21

Table 2-1. Optimal rL threshold (%) in discriminating IC, IP, and NT for each rat...3-18


Table 2-2. Discrimination performance based on rL values.....3-19

Chapter 1 Introduction



Acute ischemic cerebral stroke (AIS) comprises 80% of overall cerebral stroke and has been the major cause of socioeconomic burden in most modernized society. The main cause of AIS is occlusion of a cerebral artery, which is directly followed by hypoperfusion in the respective vascular territory[1]. At acute phase, millions of neurons begin to lose their function each minute inside the infarct core (IC)[2]. If no effective therapy is employed and early recanalization of the occluded artery does not take place, the hypoperfusion area will diminish and then turn into irreversible ischemic infarct with time. The efficacy of intravenous thrombolysis is thus closely related to the time from AIS onset to the reperfusion of the ischemic brain [3, 4] . On the other hand, reperfusion of an already infarcted brain may result in hemorrhage and malignant brain edema that cause further damage. Therefore, it is important to recognize the acute ischemic brain tissue which is still salvageable before any form of thrombolytic therapy is to be instituted. Apparently, neuroimaging plays a major role in this regard.

The diagnostic superiority of magnetic resonance imaging (MRI) for AIS has been firmly established[5]. Diffusion-weighted imaging (DWI) and perfusion-weighted imagings (PWI) are two of the most powerful techniques for AIS diagnosis and



management. DWI may delineate infarcted brain tissue within minutes[6] and PWI define the area of cerebral hypoperfusion, which is potentially salvageable from ischemic damage[7]. Recently, several multi-centric trials such as DIAS and DEFUSE began to move from computed tomography (CT) to MRI in an attempt to find other indicators, which can be utilized to tailor to the individual patient's need [8, 9]. For example, the MR-defined ischemic penumbra (IP) by lesion volume difference between PWI and DWI may potentially help to extend therapeutic time window more than 3 hours[10]. Notwithstanding, the requirements for thrombolytic therapy of recombinant tissue plasminogen activator (rtPA) haven't changed for the last 20 years, i.e. the documentation of a National Institutes of Health Stroke Scale (HINSS) score, exclusion of intracranial hemorrhage (ICH) by CT, and AIS within the first 3 hours.[11]. One of the reasons is that using the IP or PWI/DWI mismatch as a simplified marker for thrombolysis could be very technically demanding and is not available in many institutes[12, 13]. Although perfusion and diffusion maps can be obtained separately with many MRI workstations, there are only a few tools available to compute PWI/DWI mismatch maps[14]. Therefore, without suitable software, the computation of IP is time-consuming and operator-dependent. On the other hand, nephrogenic systemic

fibrosis (NSF) associated with gadolinium-based contrast agents may prompt concerns in methods that do not require exogenous contrast agents.



More recently, diffusion tensor imaging (DTI) has shown to be capable of delineating the micro-structural changes of brain due to ischemic injury. DTI, which measures diffusion in a minimum of six directions, is better suited for a more comprehensive evaluation of diffusion changes in ischemic white matter, commonly expressed as the fractional anisotropy (FA). In early cerebral ischemia, FA value can be higher in infarcted region than that of contralateral normal brain, suggesting irreversible structural damage[15]. It is not known exactly, however, if the conversion of FA can be used as the indicator for therapeutic time window[16, 17]. On the other hand, DTI may help the determination of lesion age of AIS[18]. Therefore, it is desirable that certain functional imaging parameters such as DTI from the acute setting could be used as a surrogate marker in the decision making of acute ischemic stroke therapy. To evaluate the time course of FA as a function of IP and cell edema as shown by DWI, it is important to establish an animal model in order to simulate a transient or permanent ischemic cerebral stroke such that the evolution of the ischemic brain can be monitored by repeated scans over time. Another important issue is the need of high resolution MR

imaging with reasonable signal-to-noise (SNR) ratio if the simulations are to be performed in small animals.



In this study, we established permanent occlusion model in rat at 7T MRI and utilize the advantages of ultrahigh field MRI for a higher SNR[19], which in turn provides higher resolution imaging at a relatively small expense of scan time. Keeping identical geometric parameters and similar contrast parameters, 7T can provide better visualization of the intracranial vasculature[20] and estimation of metabolite concentrations[21] than 1.5T. We hypothesize that the evolution of DTI metric changes may differ in IP and IC regions due to different stages of axonal and myelin damages as a result of different extents of perfusion deficit during the hyperacute stroke stage. We further hypothesize that the DTI metric alternations can be used to predict the first 6.5-hour onset time of stroke. To our knowledge, this is the first study to investigate the potential utility of a single DTI sequence to substitute the conventional approach of PWI/DWI mismatch, and help the estimation of stroke-lesion age with unknown onset time.

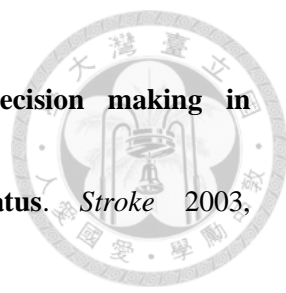



References

1. Hacke W, Schwab S, De Georgia M: **Intensive care of acute ischemic stroke.** *Cerebrovascular Diseases* 1994, **4**(6):385-392.
2. Saver JL: **Time is brain—quantified.** *Stroke* 2006, **37**(1):263-266.
3. ATLANTIS T: **Association of outcome with early stroke treatment: pooled analysis of ATLANTIS, ECASS, and NINDS rt-PA stroke trials.** *The Lancet* 2004, **363**(9411):768-774.
4. Marler JR, Tilley B, Lu M, Brott TG, Lyden P, Grotta J, Broderick J, Levine S, Frankel M, Horowitz S: **Early stroke treatment associated with better outcome The NINDS rt-PA Stroke Study.** *Neurology* 2000, **55**(11):1649-1655.
5. Chalela JA, Kidwell CS, Nentwich LM, Luby M, Butman JA, Demchuk AM, Hill MD, Patronas N, Latour L, Warach S: **Magnetic resonance imaging and computed tomography in emergency assessment of patients with suspected acute stroke: a prospective comparison.** *The Lancet* 2007, **369**(9558):293-298.
6. Fiebach J, Schellinger P, Jansen O, Meyer M, Wilde P, Bender J, Schramm P, Jüttler E, Oehler J, Hartmann M: **CT and diffusion-weighted MR imaging in randomized order Diffusion-weighted imaging results in higher accuracy and lower interrater**



- variability in the diagnosis of hyperacute ischemic stroke.** *Stroke* 2002, **33**(9):2206-2210.
7. Fink JN, Kumar S, Horkan C, Linfante I, Selim MH, Caplan LR, Schlaug G: **The stroke patient who woke up clinical and radiological features, including diffusion and perfusion MRI.** *Stroke* 2002, **33**(4):988-993.
8. Olivot J-M, Mlynash M, Thijs VN, Purushotham A, Kemp S, Lansberg MG, Wechsler L, Gold GE, Bammer R, Marks MP: **Geography, structure, and evolution of diffusion and perfusion lesions in Diffusion and perfusion imaging Evaluation For Understanding Stroke Evolution (DEFUSE).** *Stroke* 2009, **40**(10):3245-3251.
9. Marks MP, Olivot J-M, Kemp S, Lansberg MG, Bammer R, Wechsler LR, Albers GW, Thijs V: **Patients with acute stroke treated with intravenous tPA 3–6 hours after stroke onset: correlations between MR Angiography findings and perfusion-and diffusion-weighted imaging in the defuse study 1.** *Radiology* 2008, **249**(2):614-623.
10. Schellinger PD, Thomalla G, Fiehler J, Köhrmann M, Molina CA, Neumann-Haefelin T, Ribo M, Singer OC, Zaro-Weber O, Sobesky J: **MRI-based and CT-based thrombolytic therapy in acute stroke within and beyond established time windows an analysis of 1210 patients.** *Stroke* 2007, **38**(10):2640-2645.

- 
11. Schellinger PD, Fiebach JB, Hacke W: **Imaging-based decision making in thrombolytic therapy for ischemic stroke present status.** *Stroke* 2003, **34**(2):575-583.
12. Iosif C, Oppenheim C, Trystram D, Domigo V, Méder J-F: **MR imaging-based decision in thrombolytic therapy for stroke on awakening: Report of 2 cases.** *American Journal of Neuroradiology* 2008, **29**(7):1314-1316.
13. Cho A-H, Sohn S-I, Han M-K, Lee DH, Kim JS, Choi CG, Sohn C-H, Kwon SU, Suh DC, Kim SJ: **Safety and efficacy of MRI-based thrombolysis in unclear-onset stroke.** *Cerebrovascular Diseases* 2008, **25**(6):572-579.
14. Straka M, Albers GW, Bammer R: **Real-time diffusion-perfusion mismatch analysis in acute stroke.** *Journal of Magnetic Resonance Imaging* 2010, **32**(5):1024-1037.
15. Bhagat YA, Hussain MS, Stobbe RW, Butcher KS, Emery DJ, Shuaib A, Siddiqui MM, Maheshwari P, Al-Hussain F, Beaulieu C: **Elevations of diffusion anisotropy are associated with hyper-acute stroke: a serial imaging study.** *Magnetic resonance imaging* 2008, **26**(5):683-693.
16. Bhagat YA, Emery DJ, Shuaib A, Sher F, Rizvi NH, Akhtar N, Clare TL, Leatherdale T, Beaulieu C: **The relationship between diffusion anisotropy and time of onset after**

- 
- stroke**. *Journal of Cerebral Blood Flow & Metabolism* 2006, **26**(11):1442-1450.
17. Liu Y, D'Arceuil HE, Westmoreland S, He J, Duggan M, Gonzalez RG, Pryor J, De Crespigny AJ: **Serial diffusion tensor MRI after transient and permanent cerebral ischemia in nonhuman primates**. *Stroke* 2007, **38**(1):138-145.
18. Sakai K, Yamada K, Nagakane Y, Mori S, Nakagawa M, Nishimura T: **Diffusion tensor imaging may help the determination of time at onset in cerebral ischaemia**. *Journal of Neurology, Neurosurgery & Psychiatry* 2009, **80**(9):986-990.
19. Beuf O, Jaillon F, Saint-Jalmes H: **Small-animal MRI: signal-to-noise ratio comparison at 7 and 1.5 T with multiple-animal acquisition strategies**. *Magnetic Resonance Materials in Physics, Biology and Medicine* 2006, **19**(4):202-208.
20. Kang CK, Park CA, Kim KN, Hong SM, Park CW, Kim YB, Cho ZH: **Non-invasive visualization of basilar artery perforators with 7T MR angiography**. *Journal of Magnetic Resonance Imaging* 2010, **32**(3):544-550.
21. Gonen O, Liu S, Goelman G, Ratai EM, Pilkenton S, Lentz MR, González RG: **Proton MR spectroscopic imaging of rhesus macaque brain in vivo at 7T**. *Magnetic resonance in medicine* 2008, **59**(4):692-699.

Chapter 2 Methods



In this chapter, techniques of diffusion and perfusion MR imaging used in the presented study will be introduced.

2.1 Diffusion tensor imaging and the anisotropy index

Since the basic principles of diffusion-weighted imaging (DWI) were introduced in the mid-1980s [1-3], DWI has widely used in many clinical applications [4-7]. In these applications, the most successful application of DWI has been the diagnosis and characterization of acute stroke. Previous studies have reported that DWI is able to detect water diffusion abnormalities at a very early stage of the ischemic event[8], even within minutes after the onset [9, 10]. An early detection of stroke event may provide opportunities for advanced therapies within treatment time window. DWI, therefore, has become the most reliable neuroimaging tool in routine assessment of acute/subacute ischemic stroke [11].

The diffusion of water in a medium can be regarded as a random thermal motion. This phenomenon was first detected by the English botanist Robert Brownian in 1827, and therefore named 'Brownian motion'. To probe this free motion, which is on the order of several micrometers *in vivo*, a common approach is to incorporate two



additional strong gradient pulses in the spin echo pulse sequence before and after the 180° -refocusing pulse (Fig. 1-1). These additional pulses allow this pulse sequence very sensitive to molecular motion. In this section, how diffusion affects the MRI signal would be briefly introduced.

Consider a static spin whose cumulative phase shift in the presence of a magnetic field gradient is given by [12]:

$$\varphi(t) = \gamma B_0 t + \int_0^t G(t')x(t')dt' \quad (2.1)$$

where φ is the cumulative phase shift, γ is the gyromagnetic ratio, B_0 is the static B_0 -field, G is the gradient strength, and $x(t)$ is the location of a static spin at time t . The first and second terms represent the phases due to static B_0 -field and the applied field gradients, respectively. In the absence of diffusion, there will be zero phase accumulation throughout the two additional gradient pulses and then the formation of a spin echo at exactly $t=TE$. For a moving spin, a phase shift due to the displacement throughout the two additional gradient pulses at $t=TE$ is

$$\varphi(TE) = \gamma \int_{t_1}^{t_1+\delta} G(t')x(t')dt' - \gamma \int_{t_1+\Delta}^{t_1+\Delta+\delta} G(t')x(t')dt' . \quad (2.2)$$

In the case of diffusion, the displacement of each moving spin is different, and the resulting phase shifts induced by individual spin will differ. Accordingly, the incoherent



phase shifts of all spins lead ultimately to a phase dispersion and reduced spin echo amplitude at $t = TE$.

According to the Bloch-Torrey equation incorporated the effect of diffusion[13], the corresponding spin echo attenuation can be expressed as:

$$M_{(b,TE)SE} = M_0 \exp\left(-\frac{TE}{T_2}\right) \exp(-bD) \quad (2.3)$$

where the first term is the normal echo attenuation due to spin-spin relaxation, and the second term is the diffusion term. D is the diffusion coefficient, which reflects the mobility of the molecules in their micro-environment, b describes the two additional gradient pulses amplitude and timing and is given by:

$$b = \gamma^2 G^2 \delta^2 \left(\Delta - \frac{\delta}{3}\right) \quad (2.4)$$

where γ is the gyromagnetic ratio, G is the gradient strength, δ is the duration of a single gradient lobe, and Δ is time interval between the start of the first and second gradient lobes. The diffusion coefficient (D) along any direction can therefore be calculated by two measurements with and without diffusion-encoding gradients in the following equation:

$$D = -\frac{1}{b_1 - b_0} \ln\left(\frac{M(b_1)}{M(b_0)}\right) \quad (2.5)$$

Generally, maximum b_1 values applied in the stroke diffusion studies are usually in the



range of 800–1500 s/mm²[14] and b_0 is 0. The hyperintensity observed in a DWI reflects a decrease of the diffusion coefficient of water in the ischemic region[4].

However, diffusion of water molecules in biological tissues is not always free in all directions. In fact, there are barriers to free diffusion due to the presence of macromolecules, organelles, cell membrane, and other cellular and subcellular structures[15]. This causes a phenomenon known as anisotropic diffusion, which means different diffusion properties in different directions. In biological tissues such as white matter of the brain, diffusion of water molecules has a higher mobility along the axis of the fibers than in perpendicular direction. This diffusion anisotropic process can be characterized by a tensor formalism, which fully describes molecular mobility along each direction. Mathematically the diffusion tensor is a symmetric and real 3×3 matrix with six independent elements:

$$\underline{D} = \begin{bmatrix} D_{xx} & D_{xy} & D_{xz} \\ D_{yx} & D_{yy} & D_{yz} \\ D_{zx} & D_{zy} & D_{zz} \end{bmatrix} \quad (2.6)$$

where D_{xx} , D_{yy} and D_{zz} define the diffusion constants along the main axis in the reference frame, and the off-diagonal terms, D_{ij} , represent the effect of the applied field gradient along i on the random motions along j , with $i, j = x, y, z$. [16]. As the diffusion



tensor matrix is symmetric (i.e., $D_{xy} = D_{yz}$, $D_{zx} = D_{xz}$ and $D_{zy} = D_{yz}$), at least six measurements are made including along three physical axes of the MRI scanner gradients (i.e., along the x, y, z directions) and along three oblique directions — that is combinations of x and y or y and z or z and x directions. When diffusion anisotropy is considered, Eq.(2.5) then becomes[17]:

$$\ln\left(\frac{M(b_1)}{M(b_0)}\right) = -[b_{xx}D_{xx} + b_{yy}D_{yy} + b_{zz}D_{zz} + (b_{xy} + b_{yx})D_{xy} + (b_{xz} + b_{zx})D_{xz} + (b_{yz} + b_{zy})D_{yz}]$$

where

$$b_{ij} = \gamma^2 \delta^2 \left(\Delta - \frac{\delta}{3}\right) G_i G_j, \quad i, j = x, y, z \quad (2.7)$$

In practical, this MR imaging technique is referred to as diffusion tensor imaging (DTI), which acquires six non-collinear diffusion-encoding gradients pulse sequences with high b values (typically 1000 sec/mm² is used for brain) plus one without diffusion-encoding gradient (b=0), subsequently used to calculate six diffusion coefficients (D_{ij}) along six gradient directions. After performing diagonalization of tensor matrix (\underline{D}) on the basis of each pixel, the three pairs of eigenvectors and eigenvalues can be obtained as follows:

$$\underline{D}D_i = \lambda_i D_i \text{ for } i \in \{1,2,3\} \quad (2.8)$$

In the diffusion tensor model, diffusion space can be considered as an ellipsoid with



three axes which coincide to the eigenvectors ($\bar{D}_1, \bar{D}_2, \bar{D}_3$) of \underline{D} [17] and the eigenvalues ($\lambda_1, \lambda_2, \lambda_3$) are the corresponding diffusion coefficients along the three axes of the diffusion ellipsoid. If λ_1 is the largest eigenvalue as compared with λ_2 and λ_3 , its corresponding eigenvector is referred to as the principal diffusion direction (Fig. 1-2). In neural fibers, this phenomenon is quite common and principal diffusion direction of water molecules is favored along the axis of the fibers. Conversely, in a medium such as cerebral-spinal fluid within the ventricles, the three eigenvalues could be almost the same ($\lambda_1 \approx \lambda_2 \approx \lambda_3$) and this environment would be regarded as isotropic.

Once the eigenvalues of diffusion tensor is obtained, several parameters can be constituted pixel-by-pixel to characterize the amount of diffusion anisotropy and maps of derived parameters can be produced for visualization. Here, we report two commonly used indices [16, 18-22]. One is the mean diffusivity defined as:

$$\frac{Tr(\underline{D})}{3} = \frac{D_{xx} + D_{yy} + D_{zz}}{3} \quad (2.9)$$

where the trace of the diffusion tensor is given by $Tr(\underline{D}) = D_{xx} + D_{yy} + D_{zz}$. It is used to characterize the overall mean-squared displacement of molecules and the overall presence of obstacles to diffusion, i.e., the average size of the diffusion ellipsoid. The



second one is fractional anisotropy (FA) [16]:

$$FA = \sqrt{\frac{3}{2}} \frac{\sqrt{(\lambda_1 - \bar{\lambda})^2 + (\lambda_2 - \bar{\lambda})^2 + (\lambda_3 - \bar{\lambda})^2}}{\sqrt{\lambda_1^2 + \lambda_2^2 + \lambda_3^2}} \quad (2.10)$$

FA measures the fraction of the “magnitude” of \underline{D} [16] and FA is sensitive for low anisotropy value[12]. Its range is from 0 for isotropic to 1 for infinite anisotropic diffusion.

DTI has drawn much attention on clinical applications for its ability of measuring three-dimensional water diffusion. Many important applications of this technique focus on diagnosis of white matter diseases, such as white matter degeneration[23], multiple sclerosis[24], ischemic cerebral stroke[25] (Fig.1-3) and so forth. Since this technique can measure the white matter diffusion anisotropy which somewhat directly reflects the density of white matter bundles, the principal diffusion direction can be used to trace white matter fibers, which provide the connectivity of brain regions[16].

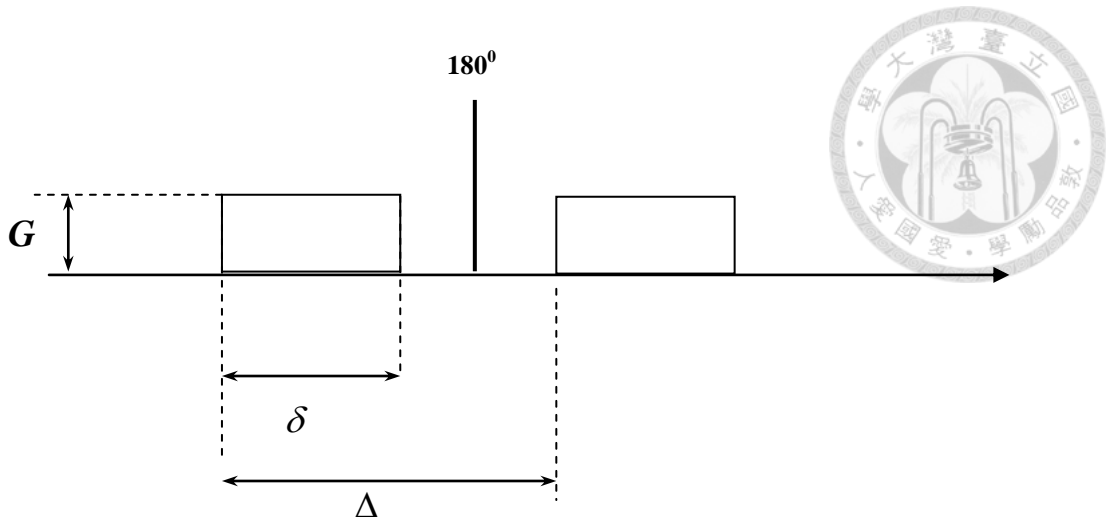


Figure 1-1. Two additional strong gradient pulses in the spin echo pulse sequence before and after the 180° -refocusing pulse. The G is the definition of the gradient strength. δ is the duration of a single gradient pulse, and Δ is time interval between the start of the first and second gradient pulses.

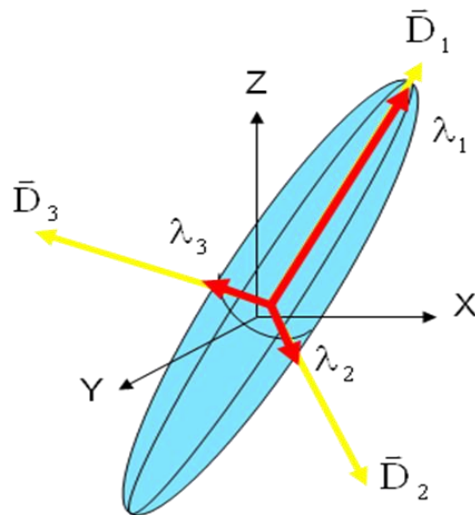


Figure 1-2. Schematic representation of diffusion ellipsoid with three axes which

coincide to the eigenvectors ($\bar{D}_1, \bar{D}_2, \bar{D}_3$) and the eigenvalues ($\lambda_1, \lambda_2, \lambda_3$).

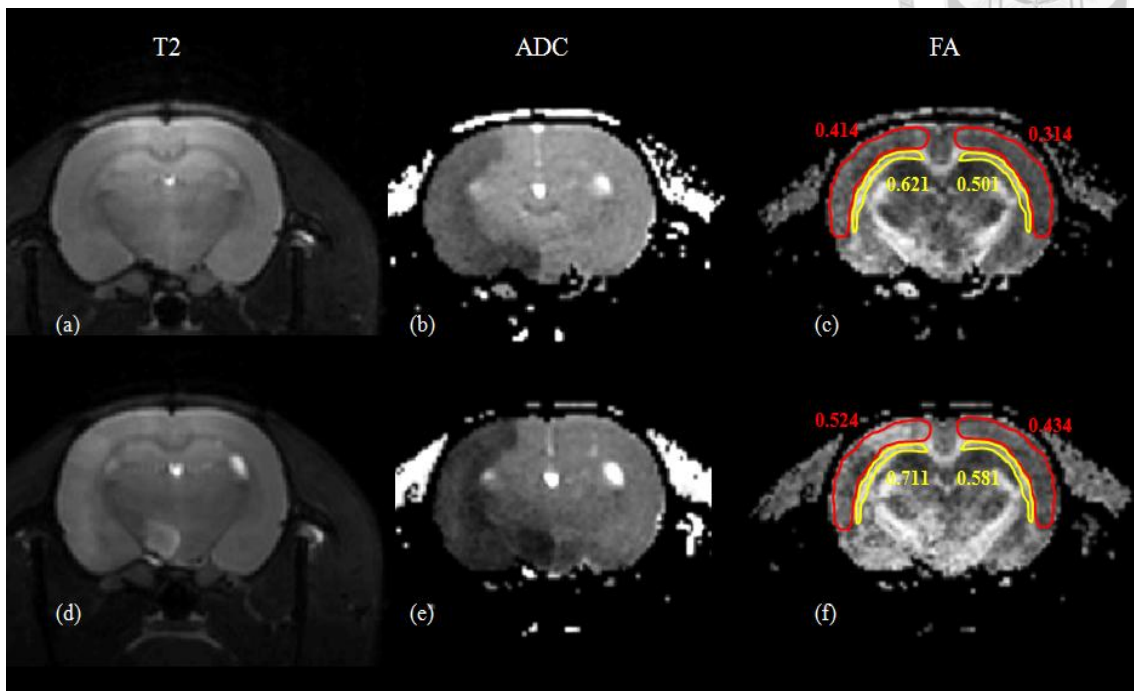


Figure 1-3. Conventional T2 image, the corresponding apparent diffusion coefficient (ADC), and FA maps of a rat stroke model at 30 minutes (a-c) and 6 hours (d-f) after onset at 7T. The red and yellow regions-of-interest are on the area of the cortices and white matter, respectively. The numbers on the FA maps represents FA values. At 30 minutes, conventional T2 image showed no obvious abnormality and the ADC map displayed signal drop on infarct region. Conversely, FA values of infarct region were higher than that of contralateral site. At 6 hours of follow-up, the conventional T2 image showed slightly hyperintense cortex and the ADC map hypointense, while FA values increased substantially in the left cortices and white matter regions.

2.2 Dynamic susceptibility contrast-enhanced technique



Various MRI techniques have been developed to measure in vivo hemodynamic parameters such as cerebral blood volume (CBV), cerebral blood flow (CBF) and mean transit time (MTT). These techniques can be categorized into two groups according to the use of contrast agents: exogenous or endogenous. In clinical practice, hemodynamic parameters are often evaluated by dynamic susceptibility-weighted contrast (DSC) MRI technique with administration of intravenous exogenous contrast agent such as gadolinium-chelate[26]. Multiple imaging levels covering the large portion of brain is acquired during the first passage of an intravenous administrated bolus agent. Because the DSC technique is based on a fast echo-planar imaging (EPI) acquisition to produce a temporal resolution of approximately 2 seconds , the whole acquisition can be accomplished less than two minutes and the maps of hemodynamic parameters can be further calculated and obtained. Rapid completion of a perfusion examination is an important consideration for uncooperative patients, such as with acute stroke or neurodegenerative diseases, which can be one of the advantages that the DSC MRI is favored in routine clinical use. However, EPI-induced distortion of anatomy is often seen due to susceptibility artifact from the skull base and orbits. In this section, we will



focus on technique of DSC MRI and introduce post-processing of the DSC data

Measurements of CBV, CBF, and MTT can be made by applying indicator dilution theory [27, 28]. Hemodynamic parameters can be quantified (i.e., expressed in absolute units) only if an arterial input function (AIF) can be measured[29]. However, quantification of hemodynamic parameters with DSC MRI may be difficult, since determination of a small diameter of the feeding arteries is problematic in a rat brain [30]. Therefore, hemodynamic parameters expressed here were semi-quantitative, termed “relative”, which indicates that no absolute quantification was performed by de-convolution with an AIF, obtaining relative CBF (rCBF), relative CBV (rCBV), and relative MTT (rMTT) in arbitrary units. In general, commercial postprocessing software packages have been widely available and easy-to-use in most modern MRI scanners.

Firstly, the acquired signal-time curve must be converted to a concentration one by the following formula[31]:

$$C(t) \propto \Delta R_2(t) = -\frac{1}{TE} \ln \frac{S(t)}{S_0} \quad (2.11)$$

where $C(t)$ is the change in concentration over time, $\Delta R_2(t)$ is the change in transverse relaxation, $S(t)$ is the signal intensity over time, S_0 is the baseline MR intensity, and TE is the echo time. In addition, to eliminate the second-pass effect (i.e., recirculation), a



gamma-variate function is used. The gamma-variate function can be expressed as[32]:

$$C(t) = k(t-t_0)^a e^{-(t-t_0)/b} \quad (2.12)$$

where k, a and b are arbitrary parameters, and t_0 is the first-bolus arrival time. The

rCBV can be determined by the integral of the post-gamma-variate fitted C(t) [33] and

rMTT can be calculated as the normalized first moment of the fitted C(t) [34] by the

following equations respectively:

$$\begin{aligned} \text{rCBV} &= \int_0^{\infty} \Delta R_2(t) dt \\ \text{rMTT} &= \frac{\int_0^{\infty} t \times \Delta R_2(t) dt}{\int_0^{\infty} \Delta R_2(t) dt} \end{aligned} \quad (2.13)$$

Using the central volume principle, rCBF can be calculated by rCBV/rMTT[35]. The

hemodynamic parameters can be calculated on a pixel-by-pixel basis and the maps

would be constituted (Fig. 1-5).

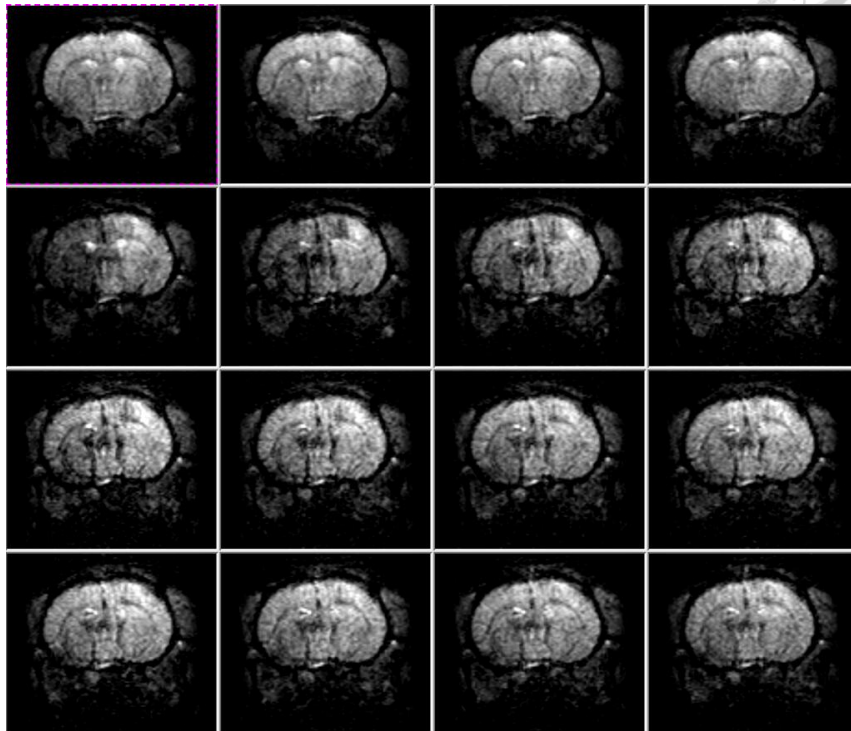


Figure 1-4. Dynamic susceptibility contrast-enhanced MR imaging of a rat brain.

Sixteen consecutive coronal images with temporal resolution of 1 second are shown from a total of 300 coronal images. The normal left hemispheres showed significant hypointensities (the second row) due to magnetic field inhomogeneity caused by the arrival of contrast agent.

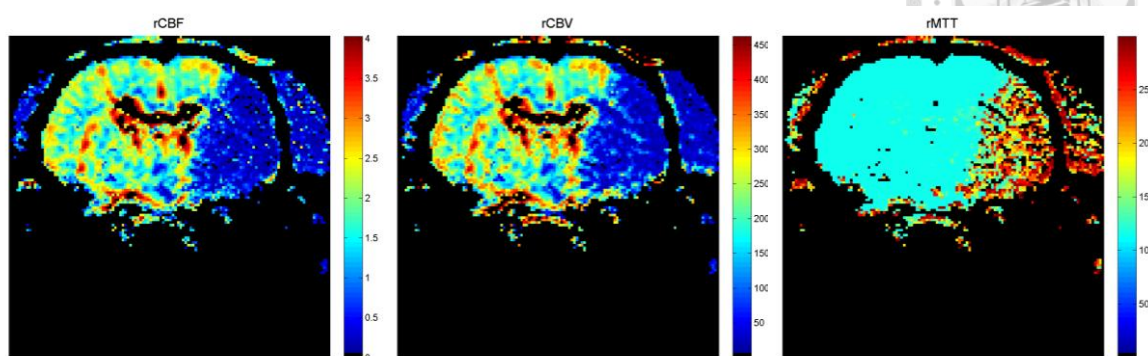


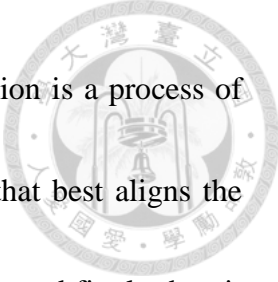
Figure 1-5. From a thread-embolized stroke rat, color-coded hemodynamic maps (from left to right: rCBF, rCBV and rMTT maps) were obtained at 2.5 hours post ischemia. On these maps, rCBF and rCBV maps showed hypointensities on right ischemic lesions, while rMTT map showed elevated values on the corresponding lesion area. The colorbars are arbitrary units.



2.3 Topographic classification of brain tissue types

Previous studies have shown variable tissue responses to the ischemic injury in cortical, subcortical gray matter (GM) and white matter (WM) [36, 37]. In this study, therefore, we applied an atlas-based classification (ABC) method during image processing to identify the tissue types within each image voxel for each rat model. The purpose of ABC method is to deform a standardized rat brain atlas into our rat's brain in order to create a new individualized rat brain atlas. To perform this, both a rat brain atlas in which the structures of interest have been previously delineated and a registration technique which find a best alignment between two images are required. In this section, a brief statement of this work is described below.

As mentioned above, the labelled rat brain atlas of Sprague-Dawley and the FA template with a isotropic resolution of 78 μm are downloaded through the INCF Software Center (Figs 1-6A and 1-6B, <http://software.incf.org/software/waxholm-space-atlas-of-the-spraguedawley-rat-brain>)[38]. The FA template will be subsequently used to co-register and resample (down-sampling) to the FA maps of rats by using the FLIRT toolbox (<https://fsl.fmrib.ox.ac.uk/fsl/fslwiki>) [39, 40]. This toolbox can be used to co-register two single image volumes together implemented by a



12-parameter affine transformation. In FLIRT, an affine transformation is a process of geometric manipulation of images in which a transforming matrix that best aligns the input (FA template) and reference (our FA map) images will be estimated firstly then it is applied to produce a new output FA map. A 3-D (a set of 2-D images) affine transformation can be achieved by using a 4×4 transforming matrix whose 12 of the 16 elements effect the operations of rotation, translation, scaling and shearing. After transforming, the original input image is resampled and a new output image is produced. The intensity of output image is derived from the input image (FA template) but the field of view (FOV) and voxel size is determined by the reference image (our FA map). In the meanwhile, the estimated matrix (i.e., 4×4 affine transforming matrix) is saved and can be secondly applied to the labelled rat brain atlas shared from the INCF Software Center to produce a new individualized one that matches the output image (Fig. 1-7).

Once the individualized labelled rat brain atlas is being completed, the tissue classification can be done accordingly. The label description file (Fig. 1-6C) can be used to specify the selected anatomical structure of interest on the atlas. In addition , the atlas originally proposed by Papp et al. differentiates the rat brain into 32 WM regions

and 40 GM regions [38]. We further categorized 37 cerebral GM regions into cortical and subcortical regions, using the corpus callosum and external capsule as the border landmarks (Fig. 1-8 and Table 1-1).



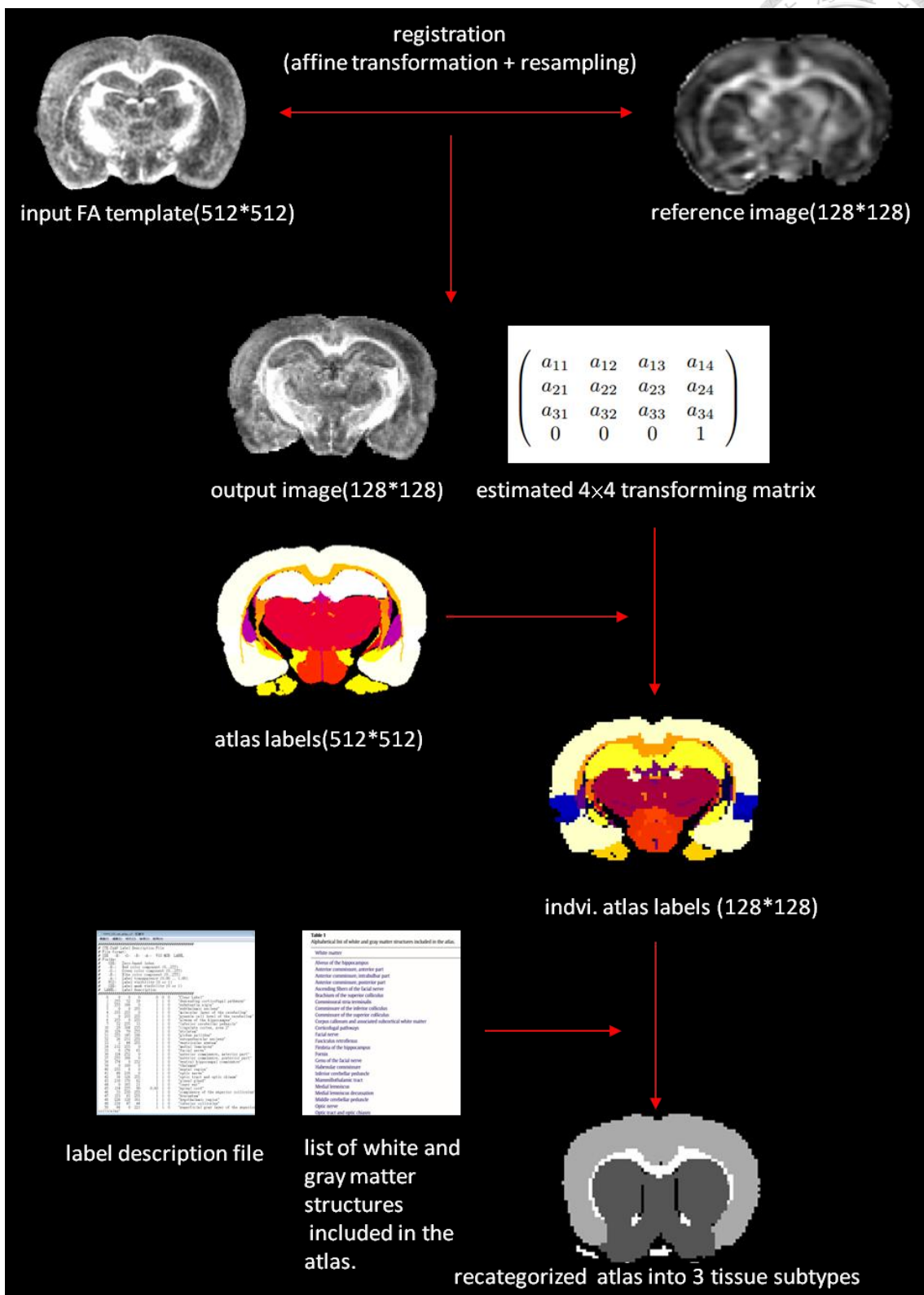


Figure 1-7. Atlas-based classification process using FLIRT toolbox

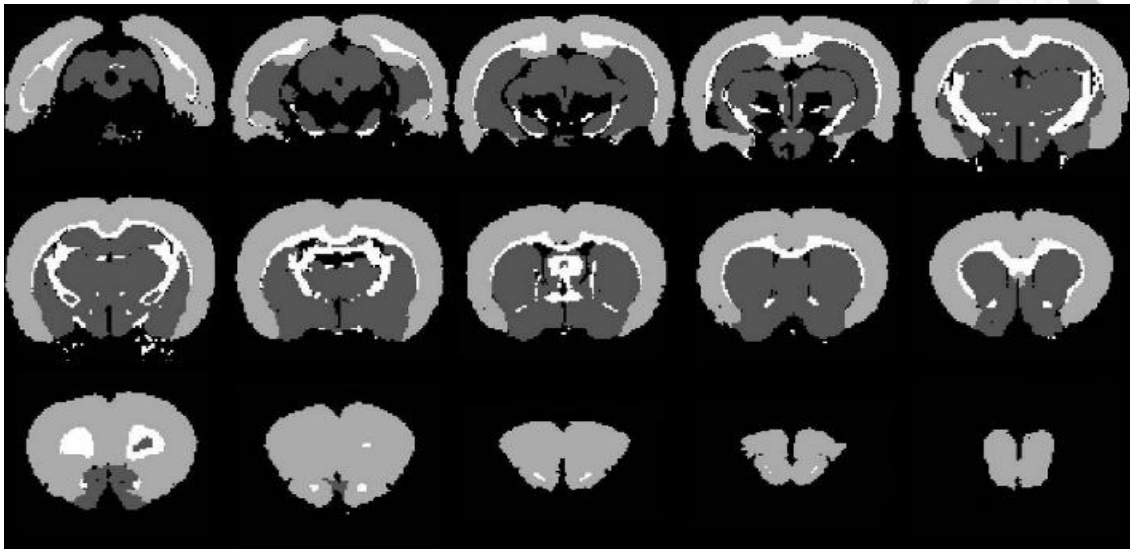


Figure 1-8. The spatial maps of identified cortical (light gray), subcortical GM (dark gray), and white matter (white).




Table 1-1. The cerebral regions defined in Sprague Dawley rat brain atlas


<i>Cortical region (gray matter)</i>	
cingulate cortex, area 2	dorsal-lateral entorhinal area
dorsal-intermediate entorhinal area	perirhinal cortex
glomerular layer of the accessory olfactory bulb	glomerular layer of the olfactory bulb
olfactory bulb	frontal association cortex
subiculum	postrhinal cortex
ventral-intermediate entorhinal area	medial entorhinal field
caudal entorhinal field	Neocortex
<i>Subcortical gray matter</i>	
substantia nigra	subthalamic nucleus
striatum	globus pallidus
entopeduncular nucleus	Thalamus
septal region	pineal gland
hypothalamic region	inferior colliculus
superficial gray layer of the superior colliculus	periaqueductal gray
deeper layers of the superior colliculus	periventricular gray
pontine nuclei	interpeduncular nucleus
inferior olive	spinal trigeminal nucleus
nucleus of the stria medullaris	basal forebrain region
hippocampal formation	bed nucleus of the stria terminalis
pretectal region	
<i>White matter</i>	
corticofugal pathways	alveus of the hippocampus
anterior commissure, intrabulbar part	medial lemniscus
facial nerve	anterior commissure, anterior part
anterior commissure, posterior part	ventral hippocampal commissure
optic nerve	optic tract and optic chiasm
commissure of the superior colliculus	Fornix
mammillothalamic tract	commissural stria terminalis
genu of the facial nerve	fimbria of the hippocampus
fasciculus retroflexus	stria medullaris of the thalamus
stria terminalis	posterior commissure
corpus callosum and associated subcortical white matter	brachium of the superior colliculus
commissure of the inferior colliculus	ascending fibers of the facial nerve
habenular commissure	supraoptic decussation



2.4 References

1. Le Bihan D, Breton E: **Imagerie de diffusion in-vivo par résonance magnétique nucléaire.** *Comptes-Rendus de l'Académie des Sciences* 1985, **93**(5):27-34.
2. Merboldt K-D, Hanicke W, Frahm J: **Self-diffusion NMR imaging using stimulated echoes.** *Journal of Magnetic Resonance (1969)* 1985, **64**(3):479-486.
3. Taylor D, Bushell M: **The spatial mapping of translational diffusion coefficients by the NMR imaging technique.** *Physics in medicine and biology* 1985, **30**(4):345.
4. Le Bihan D, Breton E, Lallemand D, Grenier P, Cabanis E, Laval-Jeantet M: **MR imaging of intravoxel incoherent motions: application to diffusion and perfusion in neurologic disorders.** *Radiology* 1986, **161**(2):401-407.
5. Assaf Y, Ben-Bashat D, Chapman J, Peled S, Biton I, Kafri M, Segev Y, Hendler T, Korczyn A, Graif M: **High b-value q-space analyzed diffusion-weighted MRI: Application to multiple sclerosis.** *Magnetic Resonance in Medicine* 2002, **47**(1):115-126.

- 
6. Hoehn - Berlage M: **Diffusion - weighted NMR imaging: application to experimental focal cerebral ischemia.** *NMR in Biomedicine* 1995, **8(7):345-358.**
 7. Hatakenaka M, Soeda H, Yabuuchi H, Matsuo Y, Kamitani T, Oda Y, Tsuneyoshi M, Honda H: **Apparent diffusion coefficients of breast tumors: clinical application.** *Magnetic Resonance in Medical Sciences* 2008, **7(1):23-29.**
 8. Moseley M, Cohen Y, Mintorovitch J, Chileuitt L, Shimizu H, Kucharczyk J, Wendland M, Weinstein P: **Early detection of regional cerebral ischemia in cats: comparison of diffusion-and T2-weighted MRI and spectroscopy.** *Magnetic resonance in medicine* 1990, **14(2):330-346.**
 9. Reith W, Hasegawa Y, Latour LL, Dardzinski BJ, Sotak CH, Fisher M: **Multislice diffusion mapping for 3-D evolution of cerebral ischemia in a rat stroke model.** *Neurology* 1995, **45(1):172-177.**
 10. Moseley M, Kucharczyk J, Mintorovitch J, Cohen Y, Kurhanewicz J, Derugin N, Asgari H, Norman D: **Diffusion-weighted MR imaging of acute stroke: correlation with T2-weighted and magnetic susceptibility-enhanced MR**


- 
- imaging in cats.** *American Journal of Neuroradiology* 1990, **11**(3):423-429.
11. Merino JG, Warach S: **Imaging of acute stroke.** *Nature Reviews Neurology* 2010, **6**(10):560-571.
 12. Bammer R: **Basic principles of diffusion-weighted imaging.** *European journal of radiology* 2003, **45**(3):169-184.
 13. Torrey HC: **Bloch equations with diffusion terms.** *Physical Review* 1956, **104**(3):563.
 14. Kim HJ, Choi CG, Lee DH, Lee JH, Kim SJ, Suh DC: **High-b-value diffusion-weighted MR imaging of hyperacute ischemic stroke at 1.5 T.** *American journal of neuroradiology* 2005, **26**(2):208-215.
 15. Le Bihan D, Basser PJ: **Molecular diffusion and nuclear magnetic resonance.** *Diffusion and perfusion magnetic resonance imaging* 1995:5-17.
 16. Le Bihan D, Mangin JF, Poupon C, Clark CA, Pappata S, Molko N, Chabriat H: **Diffusion tensor imaging: concepts and applications.** *Journal of magnetic resonance imaging* 2001, **13**(4):534-546.
 17. Basser PJ, Mattiello J, LeBihan D: **Estimation of the effective self-diffusion tensor from the NMR spin echo.** *Journal of Magnetic Resonance, Series B*

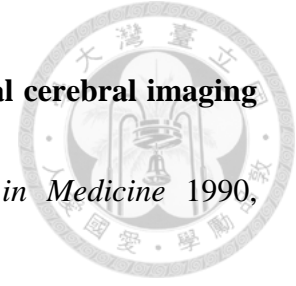


- 1994, **103**(3):247-254.
18. Zhang J, van Zijl P, Mori S: **Image contrast using the secondary and tertiary eigenvectors in diffusion tensor imaging.** *Magnetic resonance in medicine* 2006, **55**(2):439-449.
19. Song S-K, Sun S-W, Ramsbottom MJ, Chang C, Russell J, Cross AH: **Dysmyelination revealed through MRI as increased radial (but unchanged axial) diffusion of water.** *Neuroimage* 2002, **17**(3):1429-1436.
20. Song S-K, Sun S-W, Ju W-K, Lin S-J, Cross AH, Neufeld AH: **Diffusion tensor imaging detects and differentiates axon and myelin degeneration in mouse optic nerve after retinal ischemia.** *Neuroimage* 2003, **20**(3):1714-1722.
21. Sun SW, Liang HF, Trinkaus K, Cross AH, Armstrong RC, Song SK: **Noninvasive detection of cuprizone induced axonal damage and demyelination in the mouse corpus callosum.** *Magnetic Resonance in Medicine* 2006, **55**(2):302-308.
22. Basser P, Pierpaoli C: **Microstructural features measured using diffusion tensor imaging.** *J Magn Reson B* 1996, **111**(3):209-219.
23. O'Sullivan M, Jones DK, Summers P, Morris R, Williams S, Markus H:




- Evidence for cortical “disconnection” as a mechanism of age-related cognitive decline.** *Neurology* 2001, **57**(4):632-638.
24. Bammer R, Augustin M, Strasser-Fuchs S, Seifert T, Kapeller P, Stollberger R, Ebner F, Hartung HP, Fazekas F: **Magnetic resonance diffusion tensor imaging for characterizing diffuse and focal white matter abnormalities in multiple sclerosis.** *Magnetic Resonance in Medicine* 2000, **44**(4):583-591.
25. Sakai K, Yamada K, Nagakane Y, Mori S, Nakagawa M, Nishimura T: **Diffusion tensor imaging may help the determination of time at onset in cerebral ischaemia.** *Journal of Neurology, Neurosurgery & Psychiatry* 2009, **80**(9):986-990.
26. McGehee BE, Pollock JM, Maldjian JA: **Brain perfusion imaging: how does it work and what should I use?** *Journal of Magnetic Resonance Imaging* 2012, **36**(6):1257-1272.
27. Meier P, Zierler KL: **On the theory of the indicator-dilution method for measurement of blood flow and volume.** *Journal of applied physiology* 1954, **6**(12):731-744.
28. Zierler KL: **Theoretical basis of indicator-dilution methods for measuring**

- 
- flow and volume.** *Circulation Research* 1962, **10**(3):393-407.
29. Rempp KA, Brix G, Wenz F, Becker CR, Gückel F, Lorenz WJ: **Quantification of regional cerebral blood flow and volume with dynamic susceptibility contrast-enhanced MR imaging.** *Radiology* 1994, **193**(3):637-641.
30. Hofmeijer J, Schepers J, Van der Worp H, Kappelle L, Nicolay K: **Comparison of perfusion MRI by flow-sensitive alternating inversion recovery and dynamic susceptibility contrast in rats with permanent middle cerebral artery occlusion.** *NMR in Biomedicine* 2005, **18**(6):390-394.
31. Wu O, Østergaard L, Weisskoff RM, Benner T, Rosen BR, Sorensen AG: **Tracer arrival timing-insensitive technique for estimating flow in MR perfusion-weighted imaging using singular value decomposition with a block-circulant deconvolution matrix.** *Magnetic resonance in medicine* 2003, **50**(1):164-174.
32. Kluytmans M, Van der Grond J, Viergever M: **Gray matter and white matter perfusion imaging in patients with severe carotid artery lesions.** *Radiology* 1998, **209**(3):675-682.
33. Belliveau JW, Rosen BR, Kantor HL, Rzedzian RR, Kennedy DN, McKinstry



- RC, Vevea JM, Cohen MS, Pykett IL, Brady TJ: **Functional cerebral imaging by susceptibility-contrast NMR.** *Magnetic Resonance in Medicine* 1990, **14**(3):538-546.
34. Nighoghossian N, Berthezene Y, Meyer R, Cinotti L, Adeleine P, Philippon B, Froment J, Trouillas P: **Assessment of cerebrovascular reactivity by dynamic susceptibility contrast-enhanced MR imaging.** *Journal of the neurological sciences* 1997, **149**(2):171-176.
35. Nighoghossian N, Berthezene Y, Philippon B, Adeleine P, Froment J, Trouillas P: **Hemodynamic parameter assessment with dynamic susceptibility contrast magnetic resonance imaging in unilateral symptomatic internal carotid artery occlusion.** *Stroke* 1996, **27**(3):474-479.
36. Bhagat YA, Emery DJ, Shuaib A, Sher F, Rizvi NH, Akhtar N, Clare TL, Leatherdale T, Beaulieu C: **The relationship between diffusion anisotropy and time of onset after stroke.** *Journal of Cerebral Blood Flow & Metabolism* 2006, **26**(11):1442-1450.
37. Carano RA, Li F, Irie K, Helmer KG, Silva MD, Fisher M, Sotak CH: **Multispectral analysis of the temporal evolution of cerebral ischemia in the**

- 
- rat brain.** *J Magn Reson Imaging* 2000, **12**(6):842-858.
38. Papp EA, Leergaard TB, Calabrese E, Johnson GA, Bjaalie JG: **Waxholm Space atlas of the Sprague Dawley rat brain.** *Neuroimage* 2014, **97**:374-386.
39. Jenkinson M, Bannister P, Brady M, Smith S: **Improved optimization for the robust and accurate linear registration and motion correction of brain images.** *Neuroimage* 2002, **17**(2):825-841.
40. Jenkinson M, Smith S: **A global optimisation method for robust affine registration of brain images.** *Medical image analysis* 2001, **5**(2):143-156.

Chapter 3 Using DTI metrics in animal stroke model




3.1 stroke model in normobaric hyperoxia

3.1.1 Introduction

In acute ischemic stroke trial, the concept of “time is brain” is based on the non-specific computed tomography findings of possible salvageable ischemic penumbra (IP) [1]. In contrast, “physiology is brain” is another emerging concept with which the salvageable IP and infarct core (IC) can be specifically defined by perfusion/diffusion mismatch magnetic resonance imaging (MRI). However, in the acute setting, perfusion/diffusion mismatch can be both technically and computationally demanding. Moreover, in 28% of patients who had wake-up stroke, the onset time was not known [2].

Diffusion tensor imaging (DTI) can be applied to measure cerebral micro-structural changes after ischemia by characterizing their tensor magnitude, orientation, and anisotropy. The derived DTI metrics, such as fractional anisotropy (FA), can be used as surrogate markers in monitoring the cell membrane integrity over time after injuries [3]. Recent reports have indicated the advantages of DTI in determining the onset time of

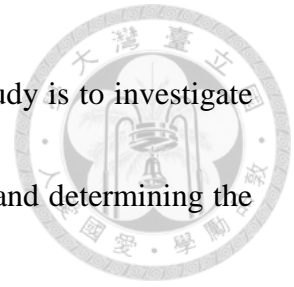


ischemic stroke, either by days or hours [4, 5]. However, these human study results were mostly extrapolated from acute data of different patients. The evolution of DTI metric changes in ischemic brain within the first 6 hours of stroke onset remains unknown.

Recent advance of high Tesla preclinical MRI has significantly improved the spatial resolution of the injured brain in ischemic stroke researches. In one murine model of permanent middle cerebral artery occlusion (MCAo), a rapid reduction of axial and radial diffusivity, along with later FA reduction at 24 hours, was consistent with axonal breakdown and myelin damage [6]. However, interpretation of ischemic injury of the microstructure solely based on FA changes can be misleading, since the FA is a relative scalar value defined by the ratio of pure anisotropic diffusion (q) and diffusion magnitude (L). Hence, inclusion of the parameters q and L may provide a more complete picture of diffusion environment in ischemic stroke.

In the experimental rat MCAo model, we hypothesize that the evolution of DTI metric changes may differ in IP and IC regions due to different stages of axonal and myelin damages as a result of different extents of perfusion deficit during the hyperacute stroke stage. We further hypothesize that the DTI metric alternations can be used to predict the

first 6.5-hour onset time of stroke. Therefore, the purpose of our study is to investigate whether the DTI metrics are capable of discriminating IP from IC, and determining the stroke onset within the first 4.5 hours.






3.1.2 Animal preparation and data analysis

Animal preparations

The experiment procedure was approved by the local Institute of Animal Care and Utilization Committee. Eleven male Sprague-Dawley rats (250-300 g; National Laboratory Animal Center, Taiwan) were prepared by permanent occlusions of unilateral MCA using the intra-luminal suture, as proposed by Chiang et al. [7]. Three of the eleven rats died within 6.5 hours after MCAo and were therefore excluded from the subsequent analysis. One of the eight included rats died after the 24-hour imaging.

Magnetic resonance imaging

All MRI animal experiments were performed in a 7T scanner (PharmaScan 70/16; Bruker, Germany). The rats were maintained under anesthesia using 1.5-2% isoflurane with an oxygen flow of 1 L/min. Rectal temperatures were maintained at 37°C by infusing warm air through the magnet bore. In accordance with methods published by Bråtane et al. [8], T2-weighted imaging (T2WI), diffusion-weighted imaging (DWI), DTI, and dynamic susceptibility contrast (DSC) perfusion imaging were performed at eight time points, starting from 0.5 hour after MCAo, then repeated every hour until 6.5 hours, with a final 24-hour imaging performed for the assessment of the final infarct



volume. Post MCAo, 100% normobaric hyperoxia (NBO) was applied using a face mask and continued for 6.5 hours, to prolong the perfusion/diffusion mismatch evolution [9]. T2WI was acquired using TR/TE of 6000/80 ms and slice thickness of 1 mm with in-plane resolution of $0.2 \times 0.2 \text{ mm}^2$. Multi-shot echo-planar imaging technique was used for DWI with b factors of 0 and 1100 s/mm^2 . DSC imaging was estimated by a bolus injection of Gd-DTPA (0.3 mmol/kg, Magnevist, Bayer Schering Pharma, Germany) with a serial gradient-echo echo-planar imaging using TR/TE of 1000/10 ms, flip angle of 90° , and 40 repetitions. DTI were acquired using multi-shot echo-planar imaging, including 6 volumes with diffusion gradients applied along 6 non-collinear orientations ($b = 1100 \text{ s/mm}^2$), and one volume without diffusion weighting [10]. The scanning parameters were TR/TE of 10,000 /23 ms, Δ/δ of 12/4 ms, and 6 averages. All data were zero-filled to generate images with a resolution of 128×128 pixels.

Data analysis

Calculation of apparent diffusion coefficient (ADC), rCBF, and FA maps

The ADC, rCBF, and FA maps at each time point were calculated using in-house MATLAB (MathWorks, Natick, MA) scripts. The ADC map was calculated using



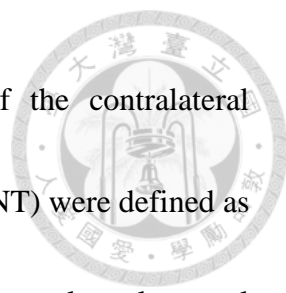
DWIs based on Stejskal-Tanner equation. For rCBF, the concentration-time curves were obtained from the signal-time curves of DSC MRI, followed by a gamma-variate fitting for the recirculation removal [11, 12]. FA maps were calculated from the DTI as follows:

$$FA = \sqrt{\frac{3}{2}} \frac{\sqrt{(\lambda_1 - \bar{\lambda})^2 + (\lambda_2 - \bar{\lambda})^2 + (\lambda_3 - \bar{\lambda})^2}}{\sqrt{\lambda_1^2 + \lambda_2^2 + \lambda_3^2}} = \sqrt{\frac{3}{2}} \frac{q}{L}$$

where λ_i were the eigenvalues of the diffusion tensor matrix, and $\bar{\lambda}$ was the mean diffusion. The scalar measures q and L represented pure diffusivity and magnitude diffusion, respectively [13].

Delineation of IP and IC

Perfusion deficit was first defined, based on the criteria that the CBF-defined lesion volume at 3 hours was equal to the infarct volume at 24 hours [14]. Because NBO can cause a reduction of CBF in normal brain and improvement of CBF in ischemic regions [9], a lower CBF threshold of 46% reduction was used in this study to identify CBF deficits [14]. Abnormal ADC was defined using a reduction of 30% of the contralateral hemisphere with the exclusion of the ventricles [9, 15]. To delineate the areas of IC and IP, the rCBF map was first co-registered to the ADC map. IP was then defined as regions showing rCBF values $< 54\%$ and ADC $> 70\%$, and IC was identified



as regions showing rCBF values < 54% and ADC < 70% of the contralateral homologous brain (Fig. 2-6). The rCBF and ADC of normal tissue (NT) were defined as the averages of the homologous areas of IP and IC values in the contralateral normal hemisphere.

Topographic classification of brain tissue types

Previous studies have shown variable tissue responses to the ischemic injury in cortical, subcortical gray matter (GM) and white matter (WM) [16, 17]. In this study, we applied an atlas-based tissue classification method during image processing to identify the tissue types within each image voxel for each rat model. Specifically, a FA template of Sprague-Dawley rat brain [18] was co-registered and resampled to the FA map of the rats using a 12-parameter affine transformation implemented by the FLIRT toolbox [19]. The tissue atlas originally proposed by Papp et al. differentiates the rat brain into 32 WM regions and 40 GM regions [18]. Further, we categorized 37 cerebral GM regions into cortical and subcortical regions, using the corpus callosum and external capsule as the border landmarks. Finally, the relative DTI metrics, as compared to the contralateral homologous tissue, were calculated as follows: $rX = (X_{\text{ipsilateral}} - X_{\text{contralateral}}) / X_{\text{contralateral}}$, where X indicates the value of indices (FA, L or q value).

Statistical Analysis

Statistical analyses were performed to determine whether the post-MCAo DTI metrics can be used to discriminate IP from IC and NT, regardless of the time effect.

One-way analysis of variance (ANOVA) model with post hoc analysis was applied to evaluate whether the means of DTI metrics within the IP, IC, and NT regions were significantly different at each imaging time point. Receiver operating characteristic (ROC) curve analysis was performed to determine the optimal threshold of rL to differentiate regions among IC, IP, and NT at 1.5 hours. The sensitivity, specificity, and accuracy were then calculated for the selected optimal thresholds. Nonlinear regression analysis using an exponential function to minimize the least squares, was employed to reveal the relationship between the rq values and the time after stroke [20].




3.1.3 Results

NBO effects on ADC and CBF lesion volumes

The evolution of IC defined by ADC lesion volume remained stationary after 90 minutes with a size around 130 mm^3 during the NBO treatment. This result indicated the effectiveness of NBO in preventing further tissue death and therefore prolonged the perfusion/diffusion mismatch. The volumes of CBF perfusion deficit were around 1.69 to 2.18 times the ADC lesion volume over the imaging time points.

Evolutions of DTI metrics among tissue types

Figure 2-1D illustrates the slight progressive increase of ischemic regions over time, on T2WI after MCAo. The L and q maps demonstrate a consistent hypointensity change in the ischemic areas over all time points (Figs. 2-1A and 2-1B). The FA maps exhibit an initial elevation of FA value at 0.5 hour in the ischemic region, and a later reduction at 6.5 hours after MCAo (Fig. 2-1C). The FA evolution depends on the changes of rL and rq values. For instance, the evolutions of rL value in IC were stagnant (with an average reduction of 41.28% and 43.25% in cortical and subcortical GM, respectively) (Fig.2-2A). However, the rq value in IC exhibited a monotonic decrease, from a reduction of 28% at 0.5 hour to 50% at 6.5 hours, in both cortical and subcortical



GM (Fig. 2-2B). Accordingly, the relatively small reduction of r_q as compared to a larger reduction of r_L resulted in a 20% increase of FA in the cortical and subcortical GM IC regions during the first 3.5 hours (Fig. 2-2C). At 6.5 hours, the reduction of r_q value became greater than the reduction of r_L , leading to a marked decrease in FA (negative rFA values) in the same region. On the other hand, the evolution of rFA in WM IC was relatively stable with a $6.41 \pm 1.34\%$ increment due to the similar decay profiles of r_L and r_q (right column in Fig. 2-2).

Discrimination of IP from IC and IP from NT by r_L

Significant differences ($p < 0.05$) in r_L values were found between IP and IC, and between IP and NT for all tissue subtypes (Fig. 2-2A). The ROC curves and the optimal r_L thresholds for discriminating IP from IC and NT are shown in Fig. 2-3, and Table 2-1, respectively. The threshold for discriminating IP from IC is relatively constant (about -29%). However, the optimal r_L threshold for separating IP from NT shows a significant difference between cortical and subcortical regions ($p = 0.022$). The results indicate that the tissue-specific r_L threshold is an important factor in discriminating between IP and NT. The overall performance of tissue-specific r_L thresholds is listed in Table 2-2, which shows excellent discrimination of IP from IC by r_L in all tissue

subtypes (average accuracy > 0.95). The discrimination performance between IP and NT is good in the subcortical GM and cortical regions, with an average accuracy of 0.83 and 0.79, respectively, and moderate in the WM region with accuracy at 0.68.

The representative maps of the rL-defined IC and IP (Fig. 2-4B) as compared with the corresponding perfusion/diffusion-defined IC and IP (Fig. 2-4A) of a rat suggested that the rL-defined maps can successfully segment the ischemic regions into IP and IC. The T2WIs at 24 hours showed complete infarct of the ipsilateral MCA territory.

Exponential decay of q-value in cortical IC

A reduction of the rq value in cortical IC from -26.9% to -47.6% within the 6.5 hours after stroke onset was observed (Fig. 2-2B). A nonlinear regression analysis was further applied to estimate the relationship between the rq values and the time after stroke. The passed time after stroke onset can be assessed by the equation, passed time (in minutes) = $1.636 \times \exp(-0.115 \times rq)$. This exponential decay of rq value over time suggests that rq value in cortical IC can be a potential surrogate marker to determine the stroke onset time at the hyperacute stage; for instance, an rq value reduction smaller than 44.6% predicts an acute stroke onset less than 4.5 hours (red dashed lines in Fig. 2-5).



3.1.4 Discussion and conclusion

Three important conclusions relating to clinical stroke management were derived from our study results: 1) The brain tissue subtypes (cortical, subcortical GM, and WM) exhibited different responses to ischemic injury, which can be characterized by the temporal evolutions of q and L ; 2) Discrimination of IP from IC and NT by rL values showed comparable results to the conventional perfusion/diffusion mismatch; 3) A reduction of 44.6% of r_q value can be used as a biomarker to determine hyperacute stroke onset at less than 4.5 hours.

Previous studies reported that NBO treatment can delay the perfusion/diffusion mismatch and improve outcome after cerebral ischemia [9, 21]. Our results confirmed the NBO effect on the prevention of further infarct in brain ischemia by illustrating a stationary evolution of ADC-defined lesion volume over time. Although the salvageable brain tissue in IP benefits from the NBO treatment, previous studies showed a limited therapeutic effect of NBO on IC [22-24]. Accordingly, monotonic decreases of r_q in IC, indicative of continuous degradations of cell membrane integrity, were observed in all cortical, subcortical GM, and WM regions under NBO. In contrast, our study showed neuroprotective effects of NBO on IP, which led to a relatively stable evolution of r_q in



IP as opposed to that in IC.

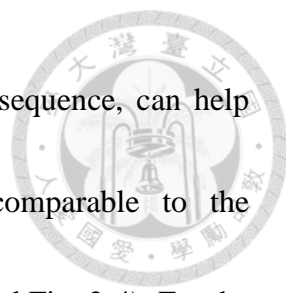
The discrepancy of anisotropy diffusion between GM and WM can be attributed to the differences in the pathophysiologic response to ischemic injury, the biophysical diffusion mechanisms, and the blood supply from collateral circulations. The pathophysiologic responses of myelinated WM to ischemia involve hydropic swelling of oligodendroglial cell bodies and the astrocytic swelling secondary to cytotoxic edema, resulting in axonal changes [25, 26]. The vulnerability of WM can lead to earlier and greater anisotropy changes than GM in acute stroke.

In biophysical diffusion mechanisms, the intra- and extracellular accumulation of fluid, and resultant changes in water diffusion, also differs between GM and WM [27, 28]. Furthermore, mechanisms of cytoskeletal breakdown and disruption of axonal transport were only observed in WM, and therefore can cause further diffusion reduction [25, 26]. Finally, the pial collateral circulation is a critical source of perfusion for the cortical GM after ischemia [29]. Previous rodent study has reported that the integrity of native pial collateral circulation is a major contributor to the tissue survival after MCAo [30]. Therefore, the existence of collateral circulation may interpret the lesser decrease of diffusion anisotropy in cortical IC (-26.89% of r_q) as compared to the

larger reduction of anisotropy in WM IC (-38.20% of r_q) at 0.5 hours after MCAo (Fig. 2B).




Perfusion/diffusion mismatch has been extensively used to individually identify the salvageable IP and IC regions in acute stroke. However, this advanced imaging technique is limited by several technical and computational demands at the acute setting. First, the injection of gadolinium-based contrast agent requires normal renal function and may potentially cause nephrogenic systemic fibrosis [31]. Second, although DSC-derived perfusion parameters correlated well with the quantitative PET findings in acute stroke [32], the DSC technique may overestimate the CBF and underestimate the mean transit time [33]. Third, several computational issues need to be carefully addressed when deriving rCBF from DSC data. Gamma-variate fitting is a necessary process to extract the first pass of the contrast agent while reducing noise contamination [11]. The rCBF estimation may be affected by the employed deconvolution model, especially in the clinical DSC data [34]. Finally, perfusion- and diffusion-weighted images are acquired by using two separate imaging sequences, and therefore post-processing to co-register two image sets are required to improve the accuracy in estimating the mismatch between ADC- and CBF-defined deficits. Our findings



suggested that the L-defined maps, calculated from a single DTI sequence, can help discriminate IP from IC (with accuracy > 0.95) which is comparable to the perfusion/diffusion mismatch during hyperacute stroke (Fig. 2-2A and Fig. 2-4). For the discrimination between IP and NT, the tissue-specific rL thresholds can ensure sufficient accuracies (> 0.79) for tissues in the subcortical GM and cortical region; however, only moderate accuracy can be achieved in the WM areas (0.68, see Table 2-2). This can be explained by the fact that the WM is a relatively scanty area in the rat brain with limited image pixels, leading to increased vulnerability to inaccuracy.

The time course of diffusion anisotropy in acute ischemic brain has been reported by several human studies [3-5, 16] and animal models [17, 24]. These studies described an elevation of FA during the hyperacute stroke phase followed by a decrease of FA in the subacute/chronic phase [3-5, 16]. Our results also showed a 20% increase of rFA in the cortical and subcortical GM IC regions during the first 3.5 hours, and a subsequent reduction to -10% at 6.5 hours after MCAo (Fig. 2-2C). The acute increase of FA in ischemic brain can be a combined effect from the increased membrane permeability [35], myelin fiber swelling [35], and the effect of signal to noise ratio on the calculation of the anisotropy indices [36]. Furthermore, in terms of mathematics, FA value is



determined by the interplay between q and L . Therefore, investigating the individual evolutions of q and L rather than their ratio, may avoid the misinterpretations of diffusion anisotropy. Our result confirmed that the acute increase of FA in the cortical and subcortical GM IC regions was due to the relatively small reduction of r_q as compared to a larger reduction of r_L . Hence, the value of r_q may provide a more accurate measure of changes in diffusion anisotropy caused by ischemic brain injury [13].

Several human studies suggested that diffusion anisotropy measured by FA might help to determine the time of onset in cerebral ischemia [4, 5]. Changes of FA were observed by extrapolating patients with different stroke ages irrespective of topography of stroke regions, and therefore the true temporal evolution of diffusion anisotropy during the hyperacute stroke could not be revealed. In our results, the evolutions of r_q value in the cortical, subcortical GM, and WM IC regions all exhibited monotonic decreases within the first 6.5 hours of stroke onset (Fig. 2-2B). By regression analysis, the stroke age of 4.5 hours can be estimated by an r_q value of -44.6% (a 44.6% reduction) in the cortical IC regions (Fig. 2-5). These findings suggest that r_q value could be useful in evaluating stroke onset time, particularly in patients with wake-up

stroke.



Several methodological concerns must be addressed in our study. First, 100% NBO was given after MCAo and continued for 6.5 hours. Although NBO treatment is helpful to evaluate the IP regions (perfusion/diffusion mismatch) by prolonging the time window, further studies are warranted to clarify if the r_q and r_L changes during hyperacute stroke under normal atmospheric conditions would produce similar results. Second, the assessment of the DTI changes for rat WM can be limited by the imaging resolution [37]. Because the area of a rat WM is much smaller than GM areas, insufficient spatial resolution may result in additional bias caused by the partial volume effect.

Our results suggested that DTI could provide a quick and reliable measure to distinguish IP from IC based on r_L values, and predict stroke age using the r_q in cortical IC during the hyperacute phase. To our knowledge, this is the first study to demonstrate the potential utility of a single DTI sequence to substitute the conventional approach of perfusion/diffusion mismatch, and help the evaluation of stroke age with unknown onset time.

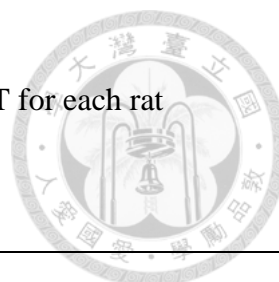


Table 2-1. Optimal rL threshold (%) in discriminating IC, IP, and NT for each rat

Rats	#1	#2	#3	#4	#5	#6	#7	#8	Average (std)
<i>IP vs. IC</i>									
Cortical	-30.01	-32.31	-29.45	-26.76	-28.70	-33.58	-27.93	-26.80	-29.44 (2.31)
Subcortical	-24.84	-29.07	-28.81	-29.02	-25.92	-28.45	-30.08	-28.07	-28.03 (1.65)
WM	-31.19	-28.28	-25.72	-27.39	-27.02	-27.25	-29.04	-32.34	-28.53 (2.09)
<i>IP vs. NT</i>									
Cortical	-6.62	-8.74	-10.63	-13.41	-10.46	-9.43	-11.63	-10.74	-10.21 (1.89)
Subcortical	-8.36	-10.61	-14.04	-12.04	-13.15	-15.92	-12.60	-13.38	-12.51 (2.13)
WM	-10.92	-12.61	-8.50	-17.60	-10.47	-11.62	-12.22	-11.53	-11.93 (2.45)

IC = infarct core, IP = ischemic penumbra, NT = normal tissue, WM = white matter, std

= standard deviation.



Table 2-2. Discrimination performance based on rL values

	Accuracy			Sensitivity			Specificity		
	Mean	Max.	Min.	Mean	Max.	Min.	Mean	Max.	Min.
<i>IP vs. IC</i>									
Cortical	0.95	0.98	0.81	0.94	0.99	0.79	0.93	0.99	0.83
Subcortical	0.97	0.99	0.91	0.98	0.99	0.94	0.92	0.99	0.75
WM	0.95	0.97	0.91	0.94	0.98	0.81	0.93	0.99	0.88
<i>IP vs. NT</i>									
Cortical	0.79	0.87	0.70	0.42	0.63	0.22	0.95	0.98	0.86
Subcortical	0.83	0.89	0.74	0.40	0.52	0.14	0.97	0.99	0.94
WM	0.68	0.77	0.60	0.40	0.56	0.26	0.91	0.99	0.83

Note.—IC = infarct core, IP = ischemic penumbra, NT = normal tissue, WM = white matter, Max = maximum, Min = minimum, Sensitivity is calculated as the proportion of positives that the perfusion/diffusion-defined IP voxels are correctly identified as IP by using the rL values; Specificity is calculated as the proportion of negatives that the perfusion/diffusion-defined IC or NT voxels are correctly identified as IC or NT based on the rL values; Accuracy is defined as the proportion of true positives and true negatives to the overall testing voxels.

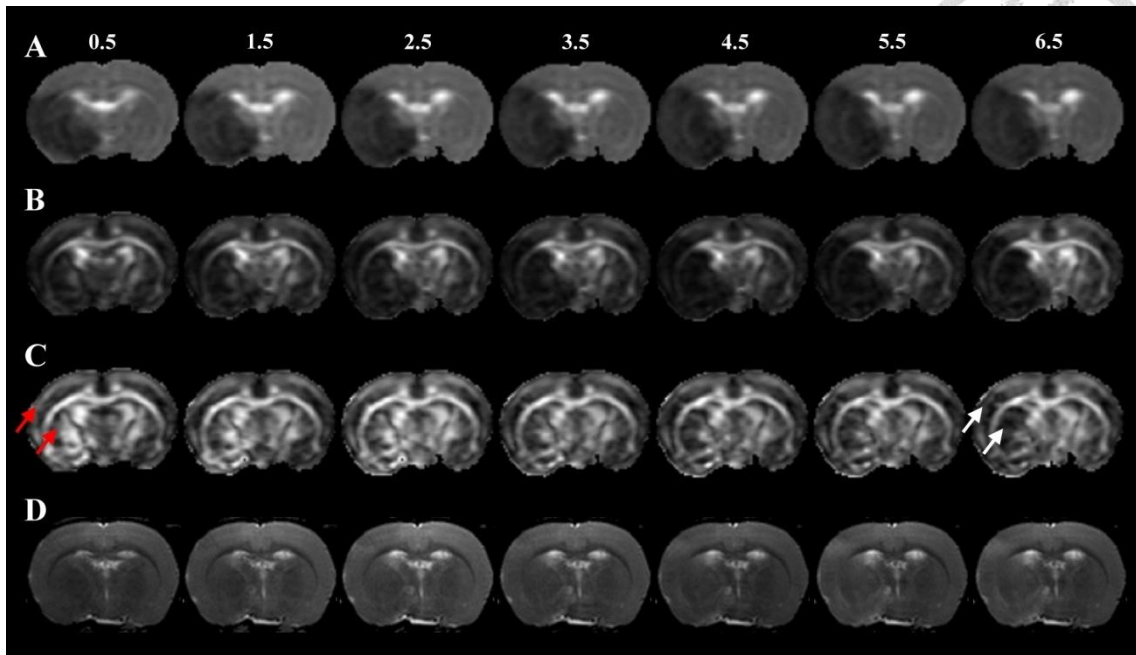


Figure 2-1. Serial L (A), q (B), FA (C), and T2WI (D) maps of a rat for demonstrating the spatiotemporal evolutions. The L and q maps showed significant hypointensities on the ischemic lesion, while FA maps displayed an initial elevation (red arrows) of the ischemia with a later reduction (white arrows) by 6.5 hours. T2WI showed progressively minor increased intensity in the ischemia areas, over time.

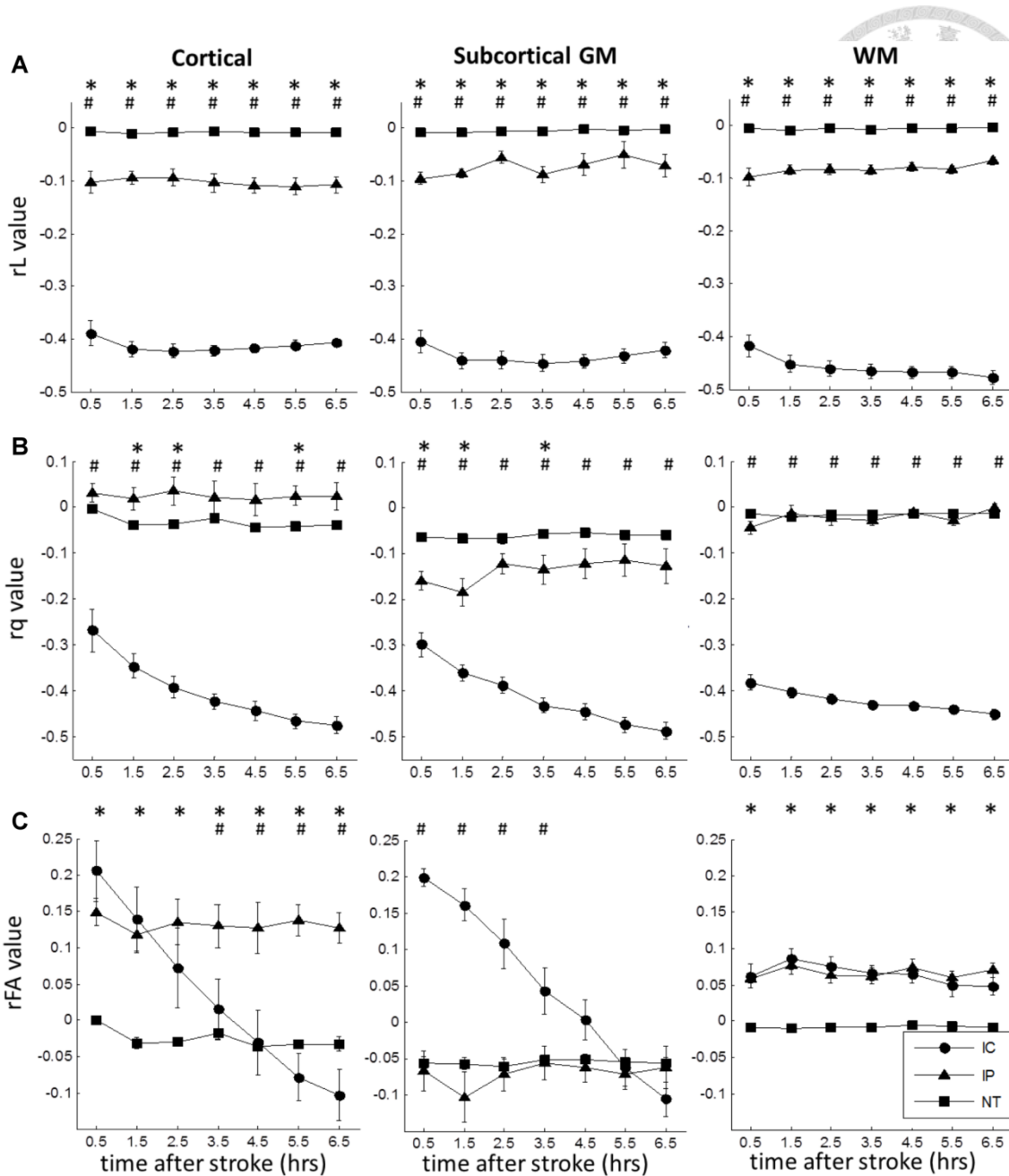


Figure 2-2. Temporal evolutions of rL (A), rq (B), and rFA (C) in cortical (left column), subcortical GM (middle column), and WM regions (right column), respectively. * indicates significant difference between IP and NT ($p < 0.05$), and # represents significant difference between IP and IC ($p < 0.05$). Error bars are \pm SEM.

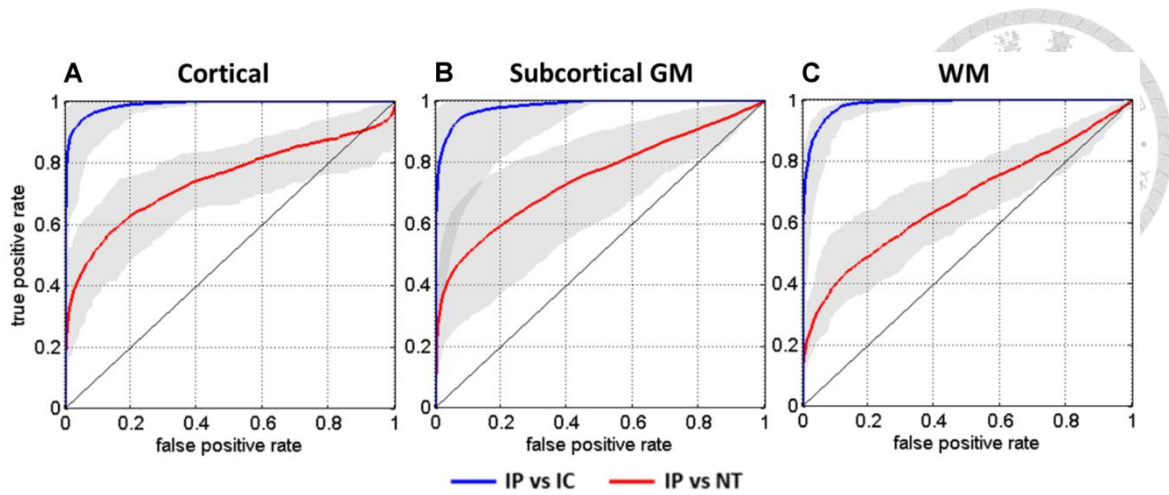


Figure 2-3. ROC curves in discriminating IP from IC (blue curves) and NT (red curves) for cortical (A), subcortical GM (B), and WM (C) using rL values. Gray areas indicate the range for eight rats.

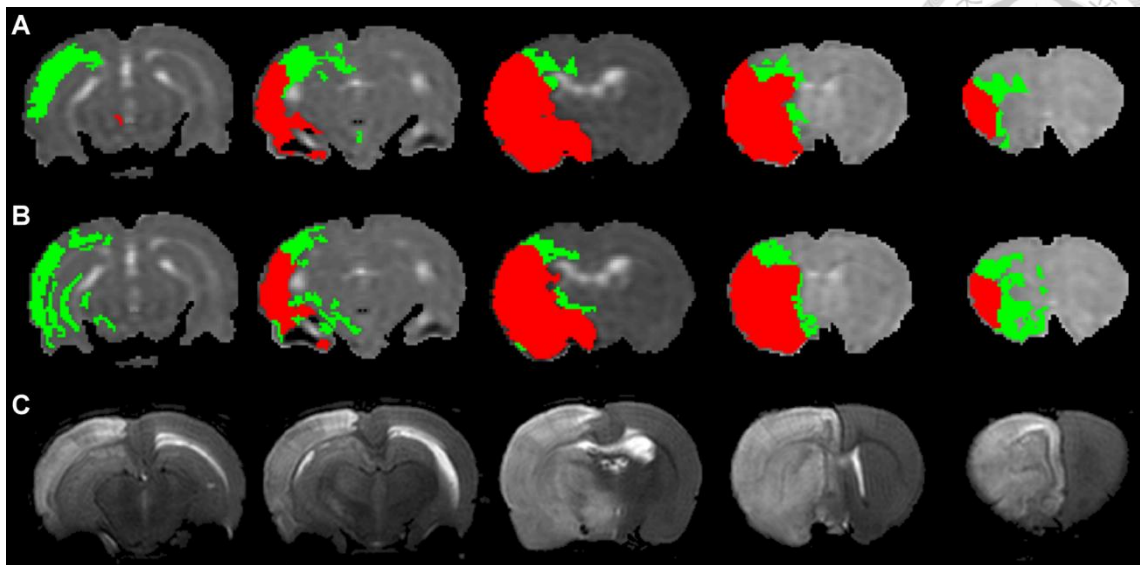


Figure 2-4. The IC (red) and IP (green) regions defined by perfusion-diffusion mismatch (**A**) and proposed L-defined method (**B**) a rat at 90 min after MCAO. The 24hr-T2WIs are also displayed to show the final infarct regions (**C**). A severe edema extending to normal hemisphere is observed in the 24hr-T2WIs.

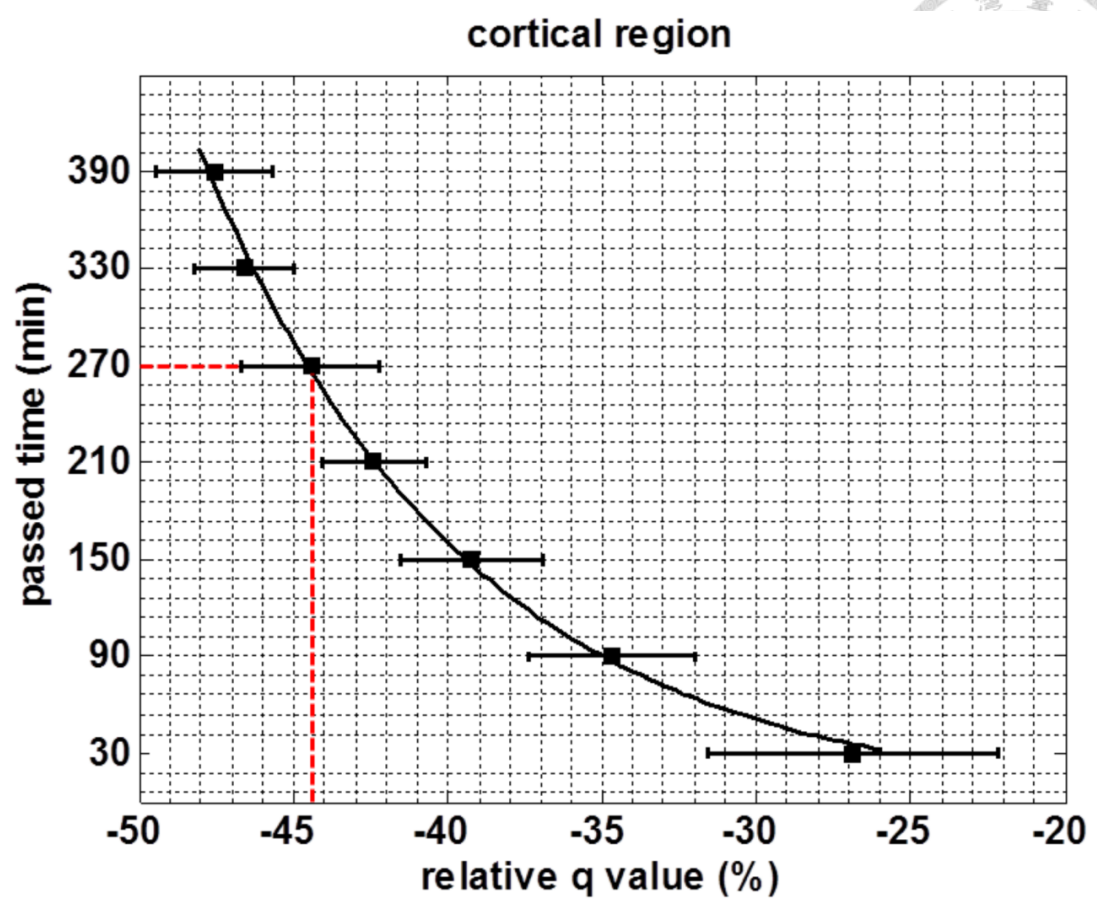
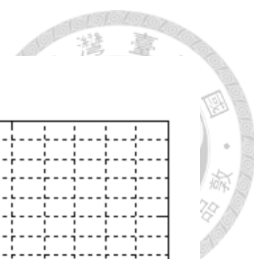


Figure 2-5. Relationship between the rq value and the time after stroke for the cortical IC. The solid curve represents the empirical relationship, i.e. elapsed time = $1.636 \cdot \exp(-0.115 \cdot \text{rq value})$, estimated by nonlinear regression analysis. The red dashed lines indicate that the 4.5-hr stroke onset can be identified by a 44.6% reduction of rq value. Error bars are \pm SEM.

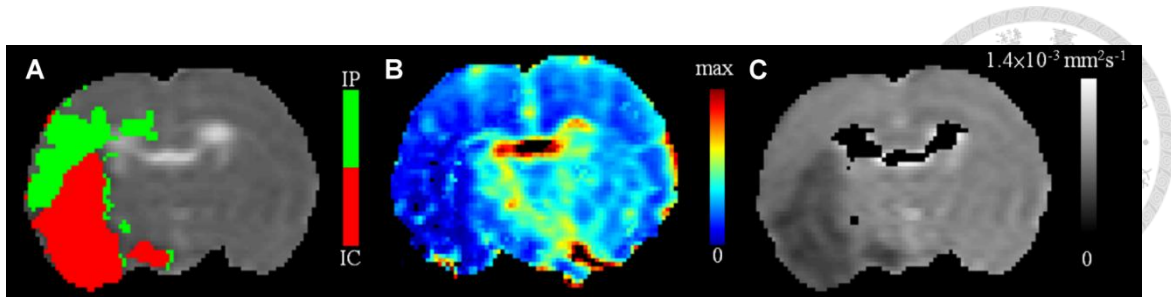
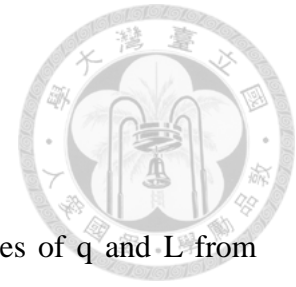


Figure 2-6. Representative perfusion/diffusion mismatch (A) by coregistration of an rCBF map (B) and an ADC map (C). The perfusion deficit was determined using a reduction of 46% of the rCBF compared to the contralateral hemisphere. Abnormal ADC was defined using a reduction of 30% of the contralateral hemisphere with the exclusion of the ventricles.

3.2 stroke model in room air



3.2.1 Introduction

In section 3.1, we have comprehensively characterized changes of q and L from different types of brain tissue in the ischemic region, using a longitudinal rat stroke model under normobaric hyperoxia (NBO). With brain tissue segmentation, the ischemic core (IC) and penumbra tissue (IP) can be successively delineated based on the tissue-specific relative L (rL) thresholds. In previous experimental design, the stroke rat under NBO can slow down the evolution of perfusion/diffusion mismatch after stroke[9], and thus “buying time” for better depict penumbra evolution during 6.5 hours. However, the use of 100 % oxygen may confuse the results and cannot be widely available to acute stroke patients. To translate our proposed tissue-specific rL thresholds for further application, herein, we repeated the experiment to investigate the evolution of q and L changes in stroke rats under room air, which closely mimics the clinical condition.



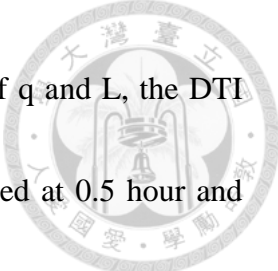
3.2.1 Animal preparation and data analysis

Animal preparations

The experiment procedure was approved by the local Institute of Animal Care and Utilization Committee. The rats were housed in a humidity- and temperature-controlled room with 12:12-hour light-dark cycle. The rats were allowed free access to sterile food and water. Sixteen male Sprague-Dawley rats (270-350 g; Taipei Medical University Animal Center, Taiwan) were prepared by permanent occlusions of unilateral MCA using the intra-luminal suture.

Magnetic resonance imaging

All MRI animal experiments were performed in a 7T scanner (PharmaScan 70/16; Bruker, Germany). The rats were maintained under anesthesia using 1.5-2% isoflurane delivering with room air during the surgery and MR experiment. Rectal temperature was maintained at around 37°C by infusing running warm water through water-bath temperature controller set outside the magnet room. The diffusion tensor imaging (DTI) was performed with six non-collinear diffusion-encoding gradients at b factor of 1200 s/mm² plus one b = 0 s/mm² T2-weighted reference. The signal readout module was a multi-shot echo-planar imaging (TR = 3000 ms, TE = 37 ms, NEX = 6) with



navigator-echo correction. To investigate the longitudinal changes of q and L , the DTI scan was executed from 0.5 to 4.5 hours. The first scan was executed at 0.5 hour and followed by the four successive scans. The sixth scan was executed at 1.5 hours and followed by the four successive scans, and then identical scan protocol was executed at 2.5 and 3.5 hours, respectively. Finally, the total twenty DTI scans were obtained for a stroke rat. Perfusion-weighted imaging (PWI) was performed using the dynamic susceptibility contrast (DSC) technique at a temporal resolution of 1 second and 300 repetitions with bolus injection of Gd-DTPA via the tail vein. Given the pharmacokinetics of gadolinium chelate in the plasma[8], PWI are acquired only at 0.5, 1.5, 2.5, and 3.5 hours, respectively. The PWI acquired at 0.5, 1.5, 2.5, and 3.5 hours were then used to calculate the mismatch at the 0.5 hour and the following four time points, the 1.5 hours and the following four time points, the 2.5 hours and the following four time points, and the 3.5 hours and the following four time points, respectively. All image data were zero-filled to generate images with a resolution of 128×128 pixels.

Data analysis

Calculation of apparent diffusion coefficient (ADC), rCBF, and FA maps

The ADC, rCBF, and FA maps at each time point were calculated using in-house



MATLAB (MathWorks, Natick, MA) scripts as details in section 3.1.2. Specifically,

both ADC and FA maps were derived from the DTI as following equations respectively:

$$\text{ADC} = \frac{\text{Tr}(\underline{D})}{3} = \frac{D_{xx} + D_{yy} + D_{zz}}{3}$$
$$\text{FA} = \sqrt{\frac{3}{2}} \frac{\sqrt{(\lambda_1 - \bar{\lambda})^2 + (\lambda_2 - \bar{\lambda})^2 + (\lambda_3 - \bar{\lambda})^2}}{\sqrt{\lambda_1^2 + \lambda_2^2 + \lambda_3^2}} = \sqrt{\frac{3}{2}} \frac{\mathbf{q}}{\mathbf{L}}$$

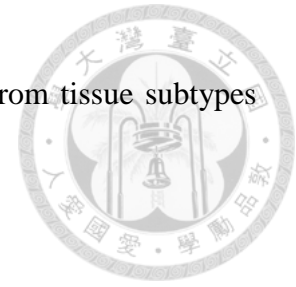
where the trace of the diffusion tensor matrix given by $\text{Tr}(\underline{D}) = D_{xx} + D_{yy} + D_{zz}$.

The λ_i were the eigenvalues of the diffusion tensor matrix, and $\bar{\lambda}$ was the mean diffusion. The scalar measures \mathbf{q} and \mathbf{L} represented pure diffusivity and magnitude diffusion, respectively [13].

Delineation of IP and IC and Tissue Segmentation

The IC and IP were defined based on the perfusion/diffusion mismatch concept, where IC was determined as tissues showing reductions of 43% or more in the relative cerebral blood flow (rCBF)[14] and a drop of 30% or more in the apparent diffusion coefficient (ADC)[15] compared with the contralateral hemisphere, and IP as tissues showing perfusion deficit but the ADC reduction was less than 30%. The normal tissue (NT) was defined as the homologous areas of IP and IC in the contralateral normal hemisphere. To identify the tissue types within each image voxel for each rat model, atlas-based tissue classification method was also applied during image processing[18].

The relative q and L , as compared to the NT, were then derived from tissue subtypes (e.g., gray matter (GM) and white matter (WM)) in ischemic region.



Statistical Analysis

Statistical analyses were performed to determine whether the post-MCAo DTI metrics can be used to discriminate IP from IC and NT, regardless of the time effect.

One-way analysis of variance (ANOVA) model with post hoc analysis was applied to evaluate whether the means of DTI metrics within the IP, IC, and NT regions were significantly different at each imaging time point.



3.2.3 Results

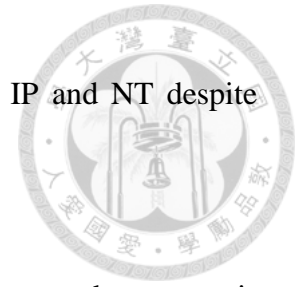
The longitudinal evolutions of q and L among tissue subtypes in IP, IC and NT, respectively, were expressed as the percentage changes relative to the contralateral tissue. After stroke onset, L values in IC dropped dramatically in all tissue subtypes at 0.5 hour (reduction of 35.73%, 35.36% and 37.74% in cortical, subcortical GM and WM, respectively, Fig. 2-7A to C) and further decreased steadily in the following 4.5 hours. While the change of L -value in IP was relative stagnant and similar among three tissue subtypes over time (reduction from 7.20 to 7.49%, 4.30 to 5.61% and 5.79 to 5.56% in the cortical, subcortical GM and WM, respectively, Fig. 2-7A to C), it is still different from NT. Reduction of q -value was found in IC among all tissue subtypes (from 12.89 to 38.01 %, from 9.74 to 32.64 % and from 32.72 to 48.84% in cortical, subcortical GM and WM, respectively, Fig. 2-8A to C), while only the change of q -value in IP in the WM was deviated from NT (increase of 0.75 to 2.07% in IP, respectively, Fig. 2-8C) after stroke.



3.2.4 Discussion and conclusion

Firstly, the results have demonstrated that the trends of post-ischemic q or L changes under room air were similar to those under NBO reported in section 3.1. Although NBO and room air groups exhibited similar behaviors of trends, animals in NBO may stop penumbral tissue migrating into infarct and then preserved more volumes of penumbra[9], which may provide advantages to reperfusion[21]. Second, the results are similar but slightly different. A possible explanation for this slight discrepancy between NBO- and room air group may lie in the contralateral normal hemisphere that was used as a reference for expressing the percentage changes of the DTI metrics due to ischemia. Although the inhalation of 100% oxygen is capable of reducing cell death in ischemic region, it also induced considerably cell death in the contralateral normal region, and the amount of dead cells within normal region appears to be larger than that under room air [9]. Neuronal death in the contralateral normal side may alter some degree of the anisotropy of neurons and their DTI metrics, leading ultimately to a slight discrepancy between NBO- and room air group. Finally, compared with NT, the magnitudes of reduction of L in IC and those in IP were significantly different at all time points (Fig. 2-7). The present findings enhanced the previous results

that L may provide a means of distinguishing regions among IC, IP and NT despite different types of tissue in the acute phase after ischemic stroke.



Taken together, the evolution of q- and L-value in stroke rats under room air showed resemble the results under NBO, which support the previous study's findings that DTI could provide a quick and reliable measure to distinguish IP from IC based on rL values, and predict stroke age using the rq in cortical IC during the hyperacute phase.

We hope that the results under room air would be helpful to translate our proposed method for further application.

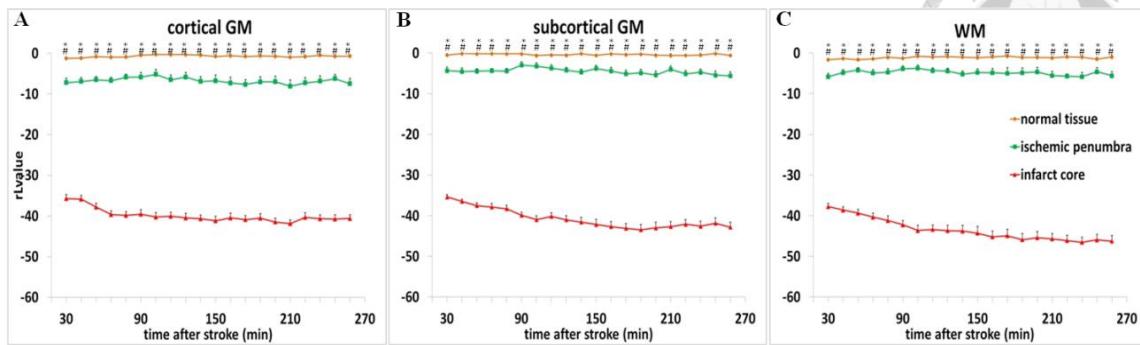


Figure 2-7. Temporal evolutions of relative L values in cortical (A), subcortical GM (B), and WM regions (C), respectively. * indicates significant difference between IP and NT ($p < 0.05$), and # represents significant difference between IP and IC ($p < 0.05$). Error bars are +SEM.

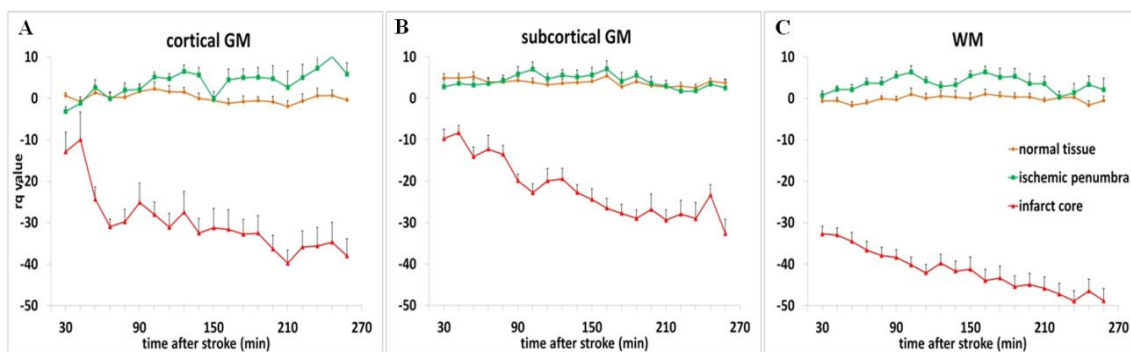


Figure 2-8. Temporal evolutions of relative q values in cortical (A), subcortical GM (B), and WM regions (C). Error bars are +SEM.



3.4 References


1. Hacke W, Kaste M, Bluhmki E, Brozman M, Dávalos A, Guidetti D, Larrue V, Lees KR, Medeghri Z, Machnig T: **Thrombolysis with alteplase 3 to 4.5 hours after acute ischemic stroke.** *New England Journal of Medicine* 2008, **359**(13):1317-1329.
2. Kang DW, Kwon JY, Kwon SU, Kim JS: **Wake-up or unclear-onset strokes: are they waking up to the world of thrombolysis therapy?** *Int J Stroke* 2012, **7**(4):311-320.
3. Bhagat YA, Hussain MS, Stobbe RW, Butcher KS, Emery DJ, Shuaib A, Siddiqui MM, Maheshwari P, Al-Hussain F, Beaulieu C: **Elevations of diffusion anisotropy are associated with hyper-acute stroke: a serial imaging study.** *Magn Reson Imaging* 2008, **26**(5):683-693.
4. Sakai K, Yamada K, Nagakane Y, Mori S, Nakagawa M, Nishimura T: **Diffusion tensor imaging may help the determination of time at onset in cerebral ischaemia.** *J Neurol Neurosurg Psychiatry* 2009, **80**(9):986-990.
5. Puig J, Blasco G, Daunis-I-Estadella J, Thomalla G, Castellanos M, Soria G, Prats-Galino A, Sánchez-González J, Boada I, Serena J: **Increased**



- Corticospinal Tract Fractional Anisotropy Can Discriminate Stroke Onset Within the First 4.5 Hours.** *Stroke* 2013, **44**(4):1162-1165.
6. Shereen A, Nemkul N, Yang D, Adhami F, Dunn RS, Hazen ML, Nakafuku M, Ning G, Lindquist DM, Kuan C-Y: **Ex vivo diffusion tensor imaging and neuropathological correlation in a murine model of hypoxia–ischemia-induced thrombotic stroke.** *Journal of Cerebral Blood Flow & Metabolism* 2011, **31**(4):1155-1169.
7. Chiang T, Messing RO, Chou W-H: **Mouse model of middle cerebral artery occlusion.** *Journal of visualized experiments: JoVE* 2011(48).
8. Bråtane BT, Walvick RP, Corot C, Lancelot E, Fisher M: **Characterization of gadolinium-based dynamic susceptibility contrast perfusion measurements in permanent and transient MCAO models with volumetric based validation by CASL.** *Journal of Cerebral Blood Flow & Metabolism* 2010, **30**(2):336-342.
9. Henninger N, Bouley J, Nelligan JM, Sicard KM, Fisher M: **Normobaric hyperoxia delays perfusion/diffusion mismatch evolution, reduces infarct volume, and differentially affects neuronal cell death pathways after suture**




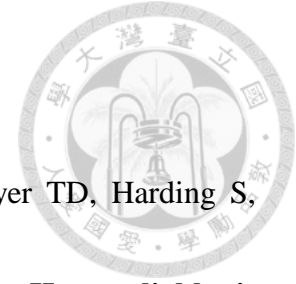
- middle cerebral artery occlusion in rats.** *Journal of Cerebral Blood Flow & Metabolism* 2007, **27**(9):1632-1642.
10. Yao X, Yu T, Liang B, Xia T, Huang Q, Zhuang S: **Effect of Increasing Diffusion Gradient Direction Number on Diffusion Tensor Imaging Fiber Tracking in the Human Brain.** *Korean J Radiol* 2015, **16**(2):410-418.
11. Østergaard L, Weisskoff RM, Chesler DA, Gyldensted C, Rosen BR: **High resolution measurement of cerebral blood flow using intravascular tracer bolus passages. Part I: Mathematical approach and statistical analysis.** *Magnetic resonance in medicine* 1996, **36**(5):715-725.
12. Lee EK, Choi SH, Yun TJ, Kang KM, Kim TM, Lee S-H, Park C-K, Park S-H, Kim IH: **Prediction of response to concurrent chemoradiotherapy with temozolomide in glioblastoma: application of immediate post-operative dynamic susceptibility contrast and diffusion-weighted MR imaging.** *Korean J Radiol* 2015, **16**(6):1341-1348.
13. Wang W, Steward C, Desmond P: **Diffusion tensor imaging in glioblastoma multiforme and brain metastases: the role of p, q, L, and fractional anisotropy.** *Am J Neuroradiol* 2009, **30**(1):203-208.

- 
14. Meng X, Fisher M, Shen Q, Sotak CH, Duong TQ: **Characterizing the diffusion/perfusion mismatch in experimental focal cerebral ischemia.** *Annals of neurology* 2004, **55**(2):207-212.
15. Shen Q, Meng X, Fisher M, Sotak CH, Duong TQ: **Pixel-by-pixel spatiotemporal progression of focal ischemia derived using quantitative perfusion and diffusion imaging.** *Journal of Cerebral Blood Flow & Metabolism* 2003, **23**(12):1479-1488.
16. Bhagat YA, Emery DJ, Shuaib A, Sher F, Rizvi NH, Akhtar N, Clare TL, Leatherdale T, Beaulieu C: **The relationship between diffusion anisotropy and time of onset after stroke.** *Journal of Cerebral Blood Flow & Metabolism* 2006, **26**(11):1442-1450.
17. Carano RA, Li F, Irie K, Helmer KG, Silva MD, Fisher M, Sotak CH: **Multispectral analysis of the temporal evolution of cerebral ischemia in the rat brain.** *J Magn Reson Imaging* 2000, **12**(6):842-858.
18. Papp EA, Leergaard TB, Calabrese E, Johnson GA, Bjaalie JG: **Waxholm Space atlas of the Sprague Dawley rat brain.** *NeuroImage* 2014, **97**:374-386.
19. Jenkinson M, Bannister P, Brady M, Smith S: **Improved optimization for the**



- robust and accurate linear registration and motion correction of brain images.** *Neuroimage* 2002, **17**(2):825-841.
20. Marquardt DW: **An algorithm for least-squares estimation of nonlinear parameters.** *Journal of the society for Industrial and Applied Mathematics* 1963, **11**(2):431-441.
21. Henninger N, Bratane BT, Bastan B, Bouley J, Fisher M: **Normobaric hyperoxia and delayed tPA treatment in a rat embolic stroke model.** *Journal of Cerebral Blood Flow & Metabolism* 2009, **29**(1):119-129.
22. Singhal AB, Benner T, Roccatagliata L, Koroshetz WJ, Schaefer PW, Lo EH, Buonanno FS, Gonzalez RG, Sorensen AG: **A pilot study of normobaric oxygen therapy in acute ischemic stroke.** *Stroke* 2005, **36**(4):797-802.
23. Kim HY, Singhal AB, Lo EH: **Normobaric hyperoxia extends the reperfusion window in focal cerebral ischemia.** *Ann Neurol* 2005, **57**(4):571-575.
24. Flynn EP, Auer RN: **Eubaric hyperoxemia and experimental cerebral infarction.** *Ann Neurol* 2002, **52**(5):566-572.
25. Yam P, Dewar D, McCulloch J: **Axonal injury caused by focal cerebral ischemia in the rat.** *Journal of neurotrauma* 1998, **15**(6):441-450.

- 
26. Dewar D, Dawson DA: **Changes of cytoskeletal protein immunostaining in myelinated fibre tracts after focal cerebral ischaemia in the rat.** *Acta neuropathologica* 1996, **93**(1):71-77.
27. Kuroiwa T, Nagaoka T, Ueki M, Yamada I, Miyasaka N, Akimoto H: **Different apparent diffusion coefficient water content correlations of gray and white matter during early ischemia.** *Stroke* 1998, **29**(4):859-865.
28. Pantoni L, Garcia JH, Gutierrez JA: **Cerebral white matter is highly vulnerable to ischemia.** *Stroke* 1996, **27**(9):1641-1647.
29. Armitage GA, Todd KG, Shuaib A, Winship IR: **Laser speckle contrast imaging of collateral blood flow during acute ischemic stroke.** *J Cereb Blood Flow Metab* 2010, **30**(8):1432-1436.
30. Zhang H, Prabhakar P, Sealock R, Faber JE: **Wide genetic variation in the native pial collateral circulation is a major determinant of variation in severity of stroke.** *Journal of Cerebral Blood Flow & Metabolism* 2010, **30**(5):923-934.
31. Cowper SE, Robin HS, Steinberg SM, Su LD, Gupta S, LeBoit PE: **Scleromyxoedema-like cutaneous diseases in renal-dialysis patients.** *The*



- Lancet* 2000, **356**(9234):1000-1001.
32. Takasawa M, Jones PS, Guadagno JV, Christensen S, Fryer TD, Harding S, Gillard JH, Williams GB, Aigbirhio FI, Warburton EA: **How reliable is perfusion MR in acute stroke? Validation and determination of the penumbra threshold against quantitative PET.** *Stroke* 2008, **39**(3):870-877.
33. Calamante F, Gadian D, Connelly A: **Quantification of perfusion using bolus tracking magnetic resonance imaging in stroke assumptions, limitations, and potential implications for clinical use.** *Stroke* 2002, **33**(4):1146-1151.
34. Wu O, Østergaard L, Weisskoff RM, Benner T, Rosen BR, Sorensen AG: **Tracer arrival timing-insensitive technique for estimating flow in MR perfusion-weighted imaging using singular value decomposition with a block-circulant deconvolution matrix.** *Magnetic resonance in medicine* 2003, **50**(1):164-174.
35. SAKAI K, YAMADA K, OOUCHI H, NISHIMURA T: **Numerical simulation model of hyperacute/acute stage white matter infarction.** *Magn Reson Med Sci* 2008, **7**(4):187-194.
36. Pierpaoli C, Basser PJ: **Toward a quantitative assessment of diffusion**



anisotropy. *Magn Reson Med* 1996, **36**(6):893-906.

37. Kim SJ, Choi CG, Kim JK, Yun S-C, Jahng G-H, Jeong H-K, Kim EJ: **Effects of MR Parameter Changes on the Quantification of Diffusion Anisotropy and Apparent Diffusion Coefficient in Diffusion Tensor Imaging: Evaluation Using a Diffusional Anisotropic Phantom.** *Korean J Radiol* 2015, **16**(2):297-303.

Chapter 4 Conclusion



In this thesis, we have demonstrated that the microstructural changes caused by ischemic brain injury can be characterized by pure DTI metrics, the diffusion magnitude (L) and pure anisotropy (q), in hyperacute stroke. The major findings of our study can be summarized as follows:

1. The evolution of FA in IC showed decrease in cortical and subcortical regions but remained relatively steady in white matter within the first 6.5 hours of stroke. The responses of brain tissue to ischemic injury appear to be topographically dependent, probably due to differential extent of collateral circulation.

2. The difference in the FA time course between IP and IC at acute stage of stroke was mainly determined by the interplay of the dynamic changes of q and L, which were varied between IC and IP.

3. The evolutions of L value were similar in IC in all tissue subtypes, showing significant initial reductions after stroke onset and then remaining steady up to 6.5 hours. The differences of L evolution in IC as opposed to that in IP may allow discrimination of IP from IC.

4. The evolution of q value in IC showed exponential decrease from -26.9% to -44.6% in cortical regions within the 4.5 hours of stroke onset. This may help to determine the age of an ischemic stroke involving cortices.

In conclusion, our study showed distinct temporal patterns of DTI metrics in IP and IC on a rat MCAo model. The difference of rL can be used to discriminate IP from IC and from NT, based on the tissue-specific thresholds. Moreover, the pure anisotropy measured by r_q in cortical IC can be potentially employed as a surrogate marker to determine the acute stroke onset time. To our knowledge, this is the first study to demonstrate the potential usage of a single DTI sequence to substitute the conventional approach of perfusion/diffusion mismatch and help the evaluation of stroke age for patients with unknown onset time.